DESY 96-122
June 1996

ISSN 0418-9833

hep-ex/9607010 12 Jul 1996

Strangeness Production in Deep-Inelastic Positron-Proton Scattering at HERA.

H1 Collaboration

Abstract

Measurements are presented of K^0 meson and Λ baryon production in deep-inelastic positron-proton scattering (DIS) in the kinematic range $10 < Q^2 < 70\,\mathrm{GeV}^2$ and $10^{-4} < x < 10^{-2}$. The measurements, obtained using the H1 detector at the HERA collider, are discussed in the light of possible mechanisms for increased strangeness production at low Bjorken-x. Comparisons of the x_F spectra, where x_F is the fractional longitudinal momentum in the hadronic centre-of-mass frame, with results from electron-positron annihilation are made. The x_F spectra and the K^0 "seagull" plot are compared with previous DIS results. The mean K^0 and Λ multiplicities are studied as a function of the centre-of-mass energy W and are observed to be consistent with a logarithmic increase with W when compared with previous measurements. A comparison of the levels of strangeness production in diffractive and non-diffractive DIS is made. An upper limit of 0.9 nb, at the 95% confidence level, is placed on the cross-section for QCD instanton induced events.

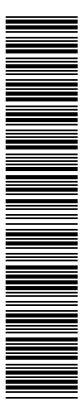

H1 Collaboration

S. Aid[13], M. Anderson[23], V. Andreev[26], B. Andrieu[29], R.-D. Appuhn[11], A. Babaev[25], J. Bähr[36], J. Bán[18], Y. Ban[28], P. Baranov[26], E. Barrelet[30], R. Barschke[11], W. Bartel[11], M. Barth[4], U. Bassler[30], [14], H.-J. Behrend[11], A. Belousov[26], Ch. Berger[1], G. Bernardi[30], G. Bertrand-Coremans[4], M. Besançon[9], R. Beyer[11], P. Biddulph[23], P. Bispham[23], J.C. Bizot[28], V. Blobel[13], K. Borras[8], F. Botterweck[4], V. Boudry[29], A. Braemer[15], W. Braunschweig[1], V. Brisson[28], P. Bruel[29], D. Bruncko[18], C. Brune[16], R. Buchholz[11], L. Büngener[13], J. Bürger[11], F.W. Büsser[13], A. Buniatian[4,39], S. Burke[19], M.J. Burton[23], D. Calvet[24], A.J. Campbell[11], T. Carli[27], M. Charlet[11], D. Clarke[5], A.B. Clegg[19], B. Clerbaux[4], S. Cocks[20], J.G. Contreras[8], C. Cormack[20], J.A. Coughlan[5], A. Courau[28], M.-C. Cousinou[24], G. Cozzika[9], L. Criegee[11], D.G. Cussans[5], J. Cvach[31], S. Dagoret[30], J.B. Dainton[20], W.D. Dau[17], K. Daum[35], M. David[9], C.L. Davis[19], A. De Roeck[11], E.A. De Wolf[4], B. Delcourt[28], P. Di Nezza[33], M. Dirkmann[8], P. Dixon[19], W. Dlugosz[7], C. Dollfus[38], J.D. Dowell[3], H.B. Dreis[2], A. Droutskoi[25], O. Dünger[13], H. Duhm[12], J. Ebert[35], T.R. Ebert[20], G. Eckerlin[11], V. Efremenko[25], S. Egli[38], R. Eichler[37], F. Eisele[15], E. Eisenhandler[21], E. Elsen[11], M. Erdmann[15], W. Erdmann[37], E. Evrard[4], A.B. Fahr[13], L. Favart[28], A. Fedotov[25], D. Feeken[13], R. Felst[11], J. Feltesse[9], J. Ferencei[18], F. Ferrarotto[33], K. Flamm[11], M. Fleischer[8], M. Flieser[27], G. Flügge[2], A. Fomenko[26], B. Fominykh[25], J. Formánek[32], J.M. Foster[23], G. Franke[11], E. Fretwurst[12], E. Gabathuler[20], K. Gabathuler[34], F. Gaede[27], J. Garvey[3], J. Gayler[11], M. Gebauer[36], H. Genzel[1], R. Gerhards[11], A. Glazov[36], U. Goerlach[11], L. Goerlich[6], N. Gogitidze[26], M. Goldberg[30], D. Goldner[8], K. Golec-Biernat[6], B. Gonzalez-Pineiro[30], I. Gorelov[25], C. Grab[37], H. Grässler[2], T. Greenshaw[20], R.K. Griffiths[21], G. Grindhammer[27], A. Gruber[27], C. Gruber[17], J. Haack[36], T. Hadig[1], D. Haidt[11], L. Hajduk[6], M. Hampel[1], W.J. Haynes[5], G. Heinzelmann[13], R.C.W. Henderson[19], H. Henschel[36], I. Herynek[31], M.F. Hess[27], K. Hewitt[3], W. Hildesheim[11], K.H. Hiller[36], C.D. Hilton[23], J. Hladký[31], K.C. Hoeger[23], M. Höppner[8], D. Hoffmann[11], T. Holtom[20], R. Horisberger[34], V.L. Hudgson[3], M. Hütte[8], M. Ibbotson[23], H. Itterbeck[1], A. Jacholkowska[28], C. Jacobsson[22], M. Jaffre[28], J. Janoth[16], T. Jansen[11], L. Jönsson[22], D.P. Johnson[4], H. Jung[9], P.I.P. Kalmus[21], M. Kander[11], D. Kant[21], R. Kaschowitz[2], U. Kathage[17], J. Katzy[15], H.H. Kaufmann[36], O. Kaufmann[15], S. Kazarian[11], I.R. Kenyon[3], S. Kermiche[24], C. Keuker[1], C. Kiesling[27], M. Klein[36], C. Kleinwort[11], G. Knies[11], T. Köhler[1], J.H. Köhne[27], F. Kole[7], S.D. Kolya[23], V. Korbel[11], M. Korn[8], P. Kostka[36], S.K. Kotelnikov[26], T. Krämerkämper[8], M.W. Krasny[6,30], H. Krehbiel[11], D. Krücker[27], H. Küster[22], M. Kuhlen[27], T. Kurča[36], J. Kurzhöfer[8], D. Lacour[30], B. Laforge[9], R. Lander[7], M.P.J. Landon[21], W. Lange[36], U. Langenegger[37], J.-F. Laporte[9], A. Lebedev[26], F. Lehner[11], S. Levonian[29], G. Lindström[12], M. Lindstroem[22], J. Link[7], F. Linsel[11], J. Lipinski[13], B. List[11], G. Lobo[28], J.W. Lomas[23], G.C. Lopez[12], V. Lubimov[25], D. Lüke[8,11], N. Magnussen[35], E. Malinovski[26], S. Mani[7], R. Maraček[18], P. Marage[4], J. Marks[24], R. Marshall[23], J. Martens[35], G. Martin[13], R. Martin[20], H.-U. Martyn[1], J. Martyniak[6], T. Mavroidis[21], S.J. Maxfield[20], S.J. McMahon[20], A. Mehta[5], K. Meier[16], A. Meyer[11], A. Meyer[13], H. Meyer[35], J. Meyer[11], P.-O. Meyer[2], A. Migliori[29], S. Mikocki[6], D. Milstead[20], J. Moeck[27], F. Moreau[29], J.V. Morris[5], E. Mroczko[6], D. Müller[38], G. Müller[11], K. Müller[11], M. Müller[11], P. Murín[18], V. Nagovizin[25], R. Nahnhauer[36], B. Naroska[13], Th. Naumann[36], I. Négri[24], P.R. Newman[3], D. Newton[19], H.K. Nguyen[30], T.C. Nicholls[3], F. Niebergall[13], C. Niebuhr[11], Ch. Niedzballa[1], H. Niggli[37], R. Nisius[1], G. Nowak[6], G.W. Noyes[5], M. Nyberg-Werther[22], M. Oakden[20], H. Oberlack[27], J.E. Olsson[11], D. Ozerov[25], P. Palmen[2], E. Panaro[11], A. Panitch[4], C. Pascaud[28], G.D. Patel[20], H. Pawletta[2], E. Peppel[36], E. Perez[9], J.P. Phillips[20], A. Pieuchot[24], D. Pitzl[37], G. Pope[7], S. Prell[11], K. Rabbertz[1], G. Rädel[11], P. Reimer[31], S. Reinshagen[11], H. Rick[8], V. Riech[12],

J. Riedlberger[37], F. Riepenhausen[2], S. Riess[13], E. Rizvi[21], S.M. Robertson[3], P. Robmann[38], H.E. Roloff[36,†], R. Roosen[4], K. Rosenbauer[1], A. Rostovtsev[25], F. Rouse[7], C. Royon[9], K. Rüter[27], S. Rusakov[26], K. Rybicki[6], D.P.C. Sankey[5], P. Schacht[27], S. Schiek[13], S. Schleif[16], P. Schleper[15], W. von Schlippe[21], D. Schmidt[35], G. Schmidt[13], A. Schöning[11], V. Schröder[11], E. Schuhmann[27], B. Schwab[15], F. Sefkow[38], M. Seidel[12], R. Sell[11], A. Semenov[25], V. Shekelyan[11], I. Sheviakov[26], L.N. Shtarkov[26], G. Siegmon[17], U. Siewert[17], Y. Sirois[29], I.O. Skillicorn[10], P. Smirnov[26], J.R. Smith[7], V. Solochenko[25], Y. Soloviev[26], A. Specka[29], J. Spiekermann[8], S. Spielman[29], H. Spitzer[13], F. Squinabol[28], M. Steenbock[13], P. Steffen[11], R. Steinberg[2], H. Steiner[11,40], J. Steinhart[13], B. Stella[33], A. Stellberger[16], J. Stier[11], J. Stiewe[16], U. Stößlein[36], K. Stolze[36], U. Straumann[15], W. Struczinski[2], J.P. Sutton[3], S. Tapprogge[16], M. Taševský[32], V. Tchernyshov[25], S. Tchetchelnitski[25], J. Theissen[2], C. Thiebaux[29], G. Thompson[21], P. Truöl[38], G. Tsipolitis[37], J. Turnau[6], J. Tutas[15], P. Uelkes[2], A. Usik[26], S. Valkár[32], A. Valkárová[32], C. Vallée[24], P. Van Esch[4], P. Van Mechelen[4], D. Vandenplas[29], Y. Vazdik[26], P. Verrecchia[9], G. Villet[9], K. Wacker[8], A. Wagener[2], M. Wagener[34], A. Walther[8], B. Waugh[23], G. Weber[13], M. Weber[16], D. Wegener[8], A. Wegner[27], T. Wengler[15], M. Werner[15], L.R. West[3], T. Wilksen[11], S. Willard[7], M. Winde[36], G.-G. Winter[11], C. Wittek[13], M. Wobisch[2], E. Wünsch[11], J. Žáček[31], D. Zarbock[12], Z. Zhang[28], A. Zhokin[25], P. Zini[30], F. Zomer[28], J. Zsembery[9], K. Zuber[16], and M. zurNedden[38]

[1] *I. Physikalisches Institut der RWTH, Aachen, Germany*[a]
[2] *III. Physikalisches Institut der RWTH, Aachen, Germany*[a]
[3] *School of Physics and Space Research, University of Birmingham, Birmingham, UK*[b]
[4] *Inter-University Institute for High Energies ULB-VUB, Brussels; Universitaire Instelling Antwerpen, Wilrijk; Belgium*[c]
[5] *Rutherford Appleton Laboratory, Chilton, Didcot, UK*[b]
[6] *Institute for Nuclear Physics, Cracow, Poland*[d]
[7] *Physics Department and IIRPA, University of California, Davis, California, USA*[e]
[8] *Institut für Physik, Universität Dortmund, Dortmund, Germany*[a]
[9] *CEA, DSM/DAPNIA, CE-Saclay, Gif-sur-Yvette, France*
[10] *Department of Physics and Astronomy, University of Glasgow, Glasgow, UK*[b]
[11] *DESY, Hamburg, Germany*[a]
[12] *I. Institut für Expewrimentalphysik, Universität Hamburg, Hamburg, Germany*[a]
[13] *II. Institut für Experimentalphysik, Universität Hamburg, Hamburg, Germany*[a]
[14] *Max-Planck-Institut für Kernphysik, Heidelberg, Germany*[a]
[15] *Physikalisches Institut, Universität Heidelberg, Heidelberg, Germany*[a]
[16] *Institut für Hochenergiephysik, Universität Heidelberg, Heidelberg, Germany*[a]
[17] *Institut für Reine und Angewandte Kernphysik, Universität Kiel, Kiel, Germany*[a]
[18] *Institute of Experimental Physics, Slovak Academy of Sciences, Košice, Slovak Republic*[f]
[19] *School of Physics and Chemistry, University of Lancaster, Lancaster, UK*[b]
[20] *Department of Physics, University of Liverpool, Liverpool, UK*[b]
[21] *Queen Mary and Westfield College, London, UK*[b]
[22] *Physics Department, University of Lund, Lund, Sweden*[g]
[23] *Physics Department, University of Manchester, Manchester, UK*[b]
[24] *CPPM, Université d'Aix-Marseille II, IN2P3-CNRS, Marseille, France*
[25] *Institute for Theoretical and Experimental Physics, Moscow, Russia*
[26] *Lebedev Physical Institute, Moscow, Russia*[f]
[27] *Max-Planck-Institut für Physik, München, Germany*[a]
[28] *LAL, Université de Paris-Sud, IN2P3-CNRS, Orsay, France*

[29] *LPNHE, Ecole Polytechnique, IN2P3-CNRS, Palaiseau, France*
[30] *LPNHE, Universités Paris VI and VII, IN2P3-CNRS, Paris, France*
[31] *Institute of Physics, Czech Academy of Sciences, Praha, Czech Republic*[f,h]
[32] *Nuclear Center, Charles University, Praha, Czech Republic*[f,h]
[33] *INFN Roma and Dipartimento di Fisica, Universita "La Sapienza", Roma, Italy*
[34] *Paul Scherrer Institut, Villigen, Switzerland*
[35] *Fachbereich Physik, Bergische Universität Gesamthochschule Wuppertal, Wuppertal, Germany*[a]
[36] *DESY, Institut für Hochenergiephysik, Zeuthen, Germany*[a]
[37] *Institut für Teilchenphysik, ETH, Zürich, Switzerland*[i]
[38] *Physik-Institut der Universität Zürich, Zürich, Switzerland*[i]
[39] *Visitor from Yerevan Phys. Inst., Armenia*
[40] *On leave from LBL, Berkeley, USA*
† *Deceased*

[a] *Supported by the Bundesministerium für Bildung, Wissenschaft, Forschung und Technologie, FRG, under contract numbers 6AC17P, 6AC47P, 6DO57I, 6HH17P, 6HH27I, 6HD17I, 6HD27I, 6KI17P, 6MP17I, and 6WT87P*
[b] *Supported by the UK Particle Physics and Astronomy Research Council, and formerly by the UK Science and Engineering Research Council*
[c] *Supported by FNRS-NFWO, IISN-IIKW*
[d] *Supported by the Polish State Committee for Scientific Research, grant nos. 115/E-743/SPUB/P03/109/95 and 2 P03B 244 08p01, and Stiftung für Deutsch-Polnische Zusammenarbeit, project no.506/92*
[e] *Supported in part by USDOE grant DE F603 91ER40674*
[f] *Supported by the Deutsche Forschungsgemeinschaft*
[g] *Supported by the Swedish Natural Science Research Council*
[h] *Supported by GA ČR, grant no. 202/93/2423, GA AV ČR, grant no. 19095 and GA UK, grant no. 342*
[i] *Supported by the Swiss National Science Foundation*

1 Introduction

This paper describes studies of the flavour structure of the hadronic final state in deep-inelastic, neutral current, positron-proton scattering (DIS) performed using the H1 detector at the HERA collider at DESY. The scattering process is described in terms of the variables $Q^2 = -q^2$, where q is the four-momentum of the exchanged boson, $x = Q^2/2p \cdot q$ and $y = p \cdot q/p \cdot k$ where p and k are, respectively, the four-momenta of the initial state proton and electron. Results from HERA have shown that the proton structure function $F_2(x, Q^2)$ measured in DIS rises rapidly as the Bjorken variable x decreases below about $x = 10^{-2}$ [1, 2]. Here it is examined if this rise is accompanied by a change in the flavour composition of the hadronic final state, in particular the strangeness production rate, associated with either the hard interaction or the subsequent hadronisation process.

Typically in electron-positron annihilation and DIS experiments at moderate or large x the production ratios of u, d, and s quarks in the soft hadronisation process have been found to be $1 : 1 : 0.3$ [3, 4], that is $\lambda_s = 0.3$, where λ_s is the strangeness suppression factor, the ratio of s quark to u or to d quark production necessary to describe the data using the Lund string hadronisation model [5]. The partial suppression of s quark production in the hadronisation is a consequence of the relative masses of the u, d and s quarks; the mass of the c quark is such that c quarks are not produced in the hadronisation process. Most recent DIS results [6, 7, 8] favour a suppression of strangeness production stronger than that above, $\lambda_s \approx 0.2$, as does one older measurement [9], although there is a recent result which prefers the higher value of λ_s [10]. Recent electron-positron annihilation measurements [11] also tend to favour $\lambda_s \approx 0.2$, but again the experimental situation is not clear [12].

In hadron-hadron collisions the mean value of the strangeness suppression factor is about 0.3 but there is evidence for a dependence on the centre-of-mass energy, the proportion of strangeness produced rising with energy. There is also some evidence for a dependence on the region of phase space investigated [13].

HERA offers the possibility of studying strangeness production in situations similar to those prevailing in all the above processes. Hadron production in DIS in the phase space region associated with the struck quark is expected to resemble that in electron-positron annihilation. This is confirmed by recent measurements [14, 15]. The rapidity region between the struck quark and the proton remnant in DIS is likely to be similar to the central plateau in hadron-hadron collisions. A recent comparison of hadron production in photoproduction and deep-inelastic electron-proton scattering supports this possibility [16]. The proton remnant is likely to be similar to the hadron remnants in hadron-hadron scattering. The phase space region in which strange particles may be identified using the current H1 apparatus corresponds to the struck quark and central plateau regions. The broad agreement of the λ_s results obtained in electron-positron annihilation with the measurements in the struck quark and central plateau regions in DIS and the central plateau in hadron-hadron collisions suggests that the colour forces responsible for hadron production in these regions are similar. It is of interest to examine whether this similarity persists at the lowest values of x accessible at HERA.

A possible source of strangeness production levels in DIS at HERA above those expected from previous measurements is QCD instantons [17]. Instantons are expected features of both QCD and the Glashow-Weinberg-Salam (GWS) model. While the cross-section for instanton induced processes is subject to large uncertainties, the properties of the final states of instanton

induced events may be calculated. These include exciting signatures such as baryon plus lepton number non-conservation in the case of the GWS model and, analogously, non-conservation of chirality in the case of QCD. The latter signature is difficult to observe experimentally, but a further property of QCD instanton induced events, the democratic production of all kinematically allowed flavours, would lead to a measureable increase in the quantity of strangeness in the final state. The kinematics of instanton induced events is such that this excess strangeness would be produced largely in the regions of the H1 detector close to the proton remnant.

A further possible mechanism for the production of strangeness at levels above expectations based on previous measurements may come into play at low x. Although the behaviour of $F_2(x, Q^2)$ in this region can be accurately described within the framework of perturbative QCD using the Dokshitzer, Gribov, Lipatov, Altarelli and Parisi (DGLAP) evolution equations [18], it has been argued that the sharp rise in $F_2(x, Q^2)$ with decreasing x is an indication that new QCD dynamics, described by the Balitsky, Fadin, Kuraev and Lipatov (BFKL) evolution equation [19], is starting to play a role at the lowest values of x accessible to HERA [20]. If the BFKL description is appropriate it is expected that the hadronic final state will also exhibit features associated with BFKL evolution, in particular the production of an increased number of gluons with large momentum transverse to the proton in the region around the proton remnant direction [21]. There are some indications that this is indeed observed [22]. This would then imply an increased level of particle, including strange particle, production in this region. Indeed, the proportion of strange particles observed might also increase as there is some evidence that events containing energetic gluons in electron-positron annihilation contain a higher proportion of K^0 mesons than is observed in two-jet events [23].

Studies at HERA have revealed that about 10% of DIS events are diffractive in nature [24, 25]. These events exhibit a large region in rapidity, close to the proton remnant, in which there is no significant hadronic energy. It has been shown that a large proportion of them may be described in terms of deep-inelastic positron-pomeron scattering. Furthermore, measurements are in agreement with Monte Carlo simulations in which the pomeron is assumed to be an object with partonic sub-structure and suggest that the pomeron is composed predominantly of gluons [26, 27].

Describing the kinematics of diffractive deep-inelastic scattering (DDIS) using the positron-pomeron scattering picture requires the introduction of two further variables: t, the square of the four-momentum of the pomeron and $x_{I\!P}$, the proportion of the proton's four-momentum carried by the pomeron. The latter may be determined using the relationship

$$x_{I\!P} \approx \frac{M_X^2 + Q^2}{W^2 + Q^2},$$

where M_X^2 is the squared invariant mass of the photon-pomeron system and W^2 is the squared invariant mass of the complete hadronic final state. The approximation is good as long as both the squared proton mass and $|t|$ are much smaller than either Q^2 or W^2, which is the case in the kinematic region considered here. In this picture of DDIS, as the pomeron has vacuum quantum numbers, the production of flavour is expected to be democratic up to effects arising from the quark masses.

An alternative model for DDIS is based on the idea that the underlying process is electron-gluon scattering via boson-gluon fusion (BGF) followed by the randomisation of the colours of the produced quark and anti-quark [28]. The probability of this producing a colour singlet

configuration is $\frac{1}{9}$. In this case there is no colour connection between the proton remnant and the quark and anti-quark, no hadrons are produced in this region, and the above diffractive signature is observed. In this model quark flavour production is again democratic up to kinematic effects. It is of interest to examine whether the quantity of strangeness produced in DDIS events is compatible with these models of diffraction.

Also of interest is the possibility that particles containing strange quarks produced in the hard interaction may be identified. Possible interaction mechanisms are: BGF resulting in the production of an $s\overline{s}$ pair, $c\overline{c}$ production via BGF followed by decay to s quarks, and the direct interaction of the virtual boson with a strange sea quark. This may ultimately allow measurement of the gluon and strange sea contributions to proton structure.

The above considerations provide the motivation for the work reported here. Strangeness production is examined by measuring the numbers and proportions of K^0_S mesons and Λ and $\overline{\Lambda}$ baryons present in the final state of DIS interactions. In the following, K^0 is taken to refer to both K^0 and $\overline{K^0}$ and Λ to both Λ and $\overline{\Lambda}$ unless explicitly stated to the contrary.

2 The Detector

A detailed description of the H1 detector can be found in [29]. The following briefly describes the components most important to this analysis. The coordinate system used is defined to have its origin at the nominal interaction point. The z axis is chosen to be along the proton beam direction, the y axis vertical and the x axis completes the right-handed coordinate system. Where polar coordinates are used, θ is the angle with respect to the z axis and ϕ the azimuthal angle with respect to the x axis. Forward and backward refer to the positive and negative z directions respectively, hence positive pseudo-rapidities $\eta = -\ln\tan(\theta/2)$ refer to objects in the forward hemisphere.

Surrounding the positron-proton interaction region are detectors designed to measure the tracks followed by charged particles. These are the central track detector (CTD) which covers the polar angular range $15^\circ < \theta < 165^\circ$ ($2.0 > \eta > -2.0$) and the forward track detector (FTD) covering the range $7^\circ < \theta < 25^\circ$ ($2.8 > \eta > 1.5$). The CTD consists of concentric inner and outer jet drift chambers. Located at the inner radii of these chambers are multi-wire proportional chambers (MWPCs), used for triggering purposes, and further drift chambers designed to measure accurately the z position of charged particle tracks. A uniform magnetic field of 1.15 T parallel to the beam axis is maintained throughout the region containing the CTD and FTD by a superconducting solenoid (see below). This system enables the transverse momentum of a charged particle to be measured with a resolution of $\sigma_{p_T}/p_T \approx 0.009 p_T \oplus 0.015$ in the CTD (p_T in GeV/c).

The liquid argon (LAr) calorimeter [30] extends over the polar angular range $4^\circ < \theta < 154^\circ$ ($3.4 > \eta > -1.5$) and covers the entire azimuth. It consists of an electromagnetic section with lead absorbers, corresponding to a depth of between 20 and 30 radiation lengths, and a hadronic section with steel absorbers. The total depth of the calorimeter varies between 4.5 and 8 hadronic interaction lengths.

The backward electromagnetic calorimeter [31] (BEMC), which is 21.7 radiation lengths deep, covers the region $151^\circ < \theta < 176^\circ$ ($-1.4 > \eta > -3.4$). A resolution of $0.10/\sqrt{E}$ with E in GeV has been achieved for positrons. The BEMC energy scale is known to an accuracy

of 1.7%. Immediately in front of the BEMC is the backward proportional chamber (BPC) which determines the point at which the scattered positron enters the BEMC to an accuracy of 1.5 mm over the polar angle range $155^\circ < \theta < 174^\circ$ ($-1.5 > \eta > -2.9$). In conjunction with a measurement of the z coordinate of the primary interaction this leads to an accuracy of 1 mrad for the measurement of the polar angle of the scattered positron.

Behind the BEMC is a time-of-flight system (ToF) with a time resolution of about 1 ns. This enables the rejection of background events caused by the interaction of protons in the material before the H1 detector, as the particles from these events arrive at the ToF system earlier than those from interactions at the nominal vertex.

The LAr calorimeter is surrounded by a superconducting solenoid which provides the magnetic field in the region containing the track detectors.

Behind the LAr calorimeter and the BEMC is an iron/streamer tube calorimeter which serves as the return yoke for the magnetic field and detects hadronic energy leaking out of the inner calorimeters. The iron/streamer tube system also serves as a muon detector.

Surrounding the beam-pipe in the forward direction is a copper/silicon calorimeter, the Plug. This device covers the range $0.7^\circ < \theta < 3.5^\circ$ ($5.1 > \eta > 3.5$).

Outside the iron in the forward direction is a muon spectrometer which consists of a toroid magnet surrounding the beam-pipe sandwiched between two layers of drift chambers. In addition to its primary function of detecting forward-going muons this device detects tracks from the secondary interactions of particles in the range $0.2^\circ < \theta < 0.8^\circ$ ($6.6 > \eta > 5.0$). These occur in the collimators designed to shield the detector from synchrotron radiation, the forward beam-pipe and the adjoining material.

The luminosity measurement system consists of electromagnetic calorimeters placed at $z = -33$ m and $z = -103$ m [32].

3 Monte Carlo Models

Calculations of the expected rate of strangeness production in DIS are available in the form of Monte Carlo event generators. These are used here, together with a Monte Carlo simulation of the H1 detector, both to correct the measurements for the finite acceptance and resolution of the detector and to make comparisons with theoretical predictions. The standard DIS Monte Carlo generators used may be split into two classes. The first class consists of those expected to describe the hadronic final state in non-diffractive DIS (NDDIS), but which contain no explicit modelling of diffractive DIS. The second class is designed explicitly to model DDIS events. Here only one such generator is considered.

The NDDIS generators are LEPTO 6.1 [33], ARIADNE 4.03 [34] and HERWIG 5.8 [35]. These generators simulate positron-proton collisions using the leading order electroweak matrix element for the interaction of a virtual boson with a parton, including exact leading order QCD corrections. The parton distributions used are the MRS(H) set of the Durham group [36] evolved to the appropriate Q^2 using the DGLAP formalism. These parton distributions were determined using most relevant available data, including the early HERA measurements of the proton structure function $F_2(x, Q^2)$ [37, 38]. The subsequent calculation differs in the three

Parameter	Description	Default value	DELPHI value	E665 value
Parj(2)	λ_s	0.3	0.23	0.2
Parj(11)	Prob. meson has spin 1 (u, d)	0.5	0.365	0.5
Parj(12)	Prob. meson has spin 1 (s)	0.6	0.410	0.6

Table 1: Values of some JETSET hadronisation parameters associated with the production of u, d and s quarks required to give a good description of PETRA and PEP data, DELPHI and E665 data.

generators. LEPTO simulates higher order perturbative QCD effects using independent parton showers in the leading logarithm approximation to generate radiation from the partons entering and leaving the hard sub-process. The observed hadrons are then produced using the Lund string hadronisation model [5], as implemented in JETSET 7.4 [39]. Three sets of fragmentation parameters are used in JETSET in this study: the default values which give a good description of PETRA and PEP electron-positron annihilation data, those providing the best description of DELPHI electron-positron annihilation data [11] and those which best describe E665 muon-nucleon scattering data [6]. These parameters are listed in table 1. The term CDM is used to refer to a calculation in which higher order perturbative QCD effects are simulated using ARIADNE, an implementation of the Colour Dipole Model [40]. In this model gluon radiation takes place initially from the dipole formed by the colour charges separated by the hard scattering process and subsequently from the dipoles formed by the radiated gluons. Again hadronisation is done using JETSET with the above parameter sets. HERWIG simulates parton showers including both colour coherence and soft gluon interference effects. Hadronisation is simulated by the non-perturbative splitting of the gluons generated in the parton showers to create colour neutral clusters, followed by the fragmentation of those clusters.

In addition to the above, DJANGO 6.0 [41] is used to study the effects of initial state photon radiation. This Monte Carlo generator simulates the electroweak interaction using HERACLES [42] and the hadronic final state using LEPTO.

The DDIS Monte Carlo used is RAPGAP 2.1 [43]. In this generator a pomeron flux, dependent only on t and $x_{I\!P}$, is associated with the proton. The pomeron is assumed to have partonic structure which evolves with Q^2 according to the DGLAP prescription. The virtual boson interacts with a parton within the pomeron, the matrix element used being as for the NDDIS Monte Carlo generators. Further parton emission is simulated using either parton showers (RAPGAP-PS) or the Colour Dipole Model (RAPGAP-CDM) and hadronisation is performed using JETSET. In conjunction with RAPGAP only the default fragmentation parameters are used. The pomeron parton distributions chosen give a good description of the latest H1 measurements of $F_2^{D(3)}$ [44].

Calculations of the expectations for the hadronic final state of instanton induced processes are made using QCDINS [45], which is a version of HERWIG modified to generate QCD instanton induced events. The number of flavours generated in the instanton decay is determined by the available instanton sub-process centre-of-mass energy, $\sqrt{s'}$. The decay is assumed to be isotropic in that frame. The minimum value of the so-called Holy Grail function [17], which enters the expression for the cross-section for instanton induced events, is fixed to be the value it reaches at $x' = 0.2$, where $x' = Q'^2/(s' + Q'^2)$ and $Q'^2 = -q'^2$ is the negative invariant mass of the virtual quark in the instanton sub-process, see figure 1.

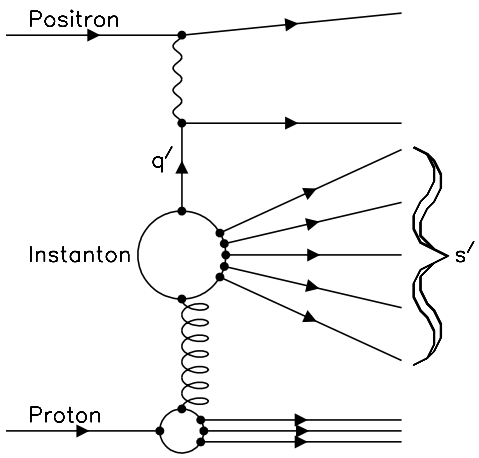

Figure 1: Diagram illustrating the kinematics of instanton induced deep-inelastic positron-proton scattering.

The number of Monte-Carlo events used in comparisons with the measurements presented in the following always exceeds the number of events in the data by a factor of three or more.

4 Data Taking and Event Selection

The data used here were collected in the 1994 running period in which 820 GeV protons and 27.5 GeV positrons were brought into head-on collision in HERA.

The trigger used in the collection of the data is the requirement that there be a localised energy deposit in the BEMC of at least 4 GeV with no associated veto signal from the ToF system. This has been shown to be more than 99% efficient for the collection of DIS events in which the scattered positron enters the BEMC and has energy greater than 10 GeV.

The events are then required to contain a localised BEMC energy deposit of at least 12 GeV spatially associated with a signal in the BPC and with a shape compatible with being due to an electromagnetic shower. It is also demanded that at least one charged particle be detected in the CTD, allowing the determination of the z coordinate of the primary interaction vertex. This is required to be within 30 cm of the z coordinate of the expected vertex position.

The polar angle of the positron candidate is required to lie in the range $156^\circ < \theta < 173^\circ$. The range in the kinematic variables studied is restricted to $10 < Q^2 < 70\,\mathrm{GeV}^2$, $10^{-4} < x < 10^{-2}$ and $0.05 < y < 0.6$, all variables being determined using the measured polar angle and energy of the scattered positron. The lower restriction in the y range ensures that these determinations are of sufficient accuracy. The above criteria are such that the boundaries of the kinematic region studied are given by the restrictions imposed on the Lorentz invariant variables Q^2, x and y. The number of events which satisfy the above is 53 360. Less than 1% of these are background

events. The largest source of background is photoproduction interactions in which one of the final state hadrons fakes the required BEMC electron signal.

The luminosity to which the data correspond is $1.32\,\mathrm{pb}^{-1}$, determined to a precision of 1.5% by studying the reaction $ep \to ep\gamma$ using the luminosity measurement system.

Similar criteria to those used to isolate DDIS events in the study of the structure of deep-inelastic diffraction [24] are used here to identify diffractive events. These are: the energy in the Plug must be less than 3 GeV; there must be fewer than 3 hit pairs in the forward muon drift chambers and the most forward significant energy deposit detected in the LAr calorimeter must be at a pseudo-rapidity of 3.0 or less. Events in which the forward-going proton remnant is separated from the centrally produced hadronic system by a rapidity gap between $\eta \sim 6.6$ and $\eta = 3.2$ and has a mass, m_R, less than $1.6\,\mathrm{GeV/c^2}$ satisfy these criteria. The DDIS event sample is restricted to the kinematic region defined by $x_{I\!P} < 0.05$ and contains 3 491 events. The variable $x_{I\!P}$ is calculated from the values of Q^2 and W^2 determined using the parameters of the scattered electron and the value of M_X obtained from the measurement of the hadronic final state.

As comparisons are made with Monte Carlo simulations which do not explicitly model the diffractive component of DIS, additional criteria are applied to select a sample of non-diffractive DIS events. These are that the events do not satisfy the diffractive selection above and in addition that the energy in the LAr calorimeter in the angular region $4.4^\circ < \theta < 15^\circ$ ($3.26 > \eta > 2.03$) exceeds 0.5 GeV. The number of events in the NDDIS sample is 46 684. The non-diffractive Monte Carlo simulations are expected to model the hadronic final state of these events. To ensure that any events produced by these simulations which fall into the DDIS category are removed, before comparisons are made with NDDIS data the Monte Carlo events are required to have a hadronic energy of at least 0.5 GeV in the above angular region.

5 K^0_S and Λ Identification

Neutral kaons are identified through the decay

$$K^0_S \to \pi^+\pi^-,$$

and Λ baryons through the decay

$$\Lambda \to p\pi^-$$

and the charge conjugate reaction. The identification utilises the separation of the decay and primary vertices arising from the relatively long K^0_S and Λ lifetimes.

The first stage in the identification of candidates for the above decays is a search for pairs of oppositely charged tracks in the CTD which originate from a vertex radially separated from the primary event vertex by at least 2 cm. Only well-measured tracks with $p_T > 0.15\,\mathrm{GeV/c}$ are considered. An attempt is made to fit these track pairs using the hypothesis that they originate from a common secondary vertex resulting from the decay of a neutral particle, generically termed a V^0, which in turn originates from the primary event vertex. The V^0 candidates which satisfy this hypothesis are then required to have transverse momenta in the range $0.25 < p_T^2 < 4.5\,(\mathrm{GeV/c})^2$ and pseudo-rapidities in the range $-1.3 < \eta < 1.3$ to ensure that they are well within the acceptance of the CTD and that the V^0 mass resolution is good.

In order to define a set of K^0_S candidates further requirements are made:

- Track pairs are required not to be Λ decay candidates. That is, it is required that the invariant mass of the track pair, $m_{p\pi}$, satisfy $m_{p\pi} > 1.125\,\mathrm{GeV/c^2}$, where the higher momentum track is assumed to be that of a proton and the lower that of a pion.

- The difference of the distance of closest approach to the primary event vertex in the transverse plane, Δd, of the tracks making up the pair is required to satisfy

$$|\Delta d| > \frac{1 + 10\exp[-p_T]}{5}\,\mathrm{cm},$$

  where p_T (in GeV/c) is the transverse momentum of the V^0 candidate. The distance of closest approach of a track, d, is given a sign that depends on the track's charge and hence large values of $|\Delta d|$ result for track pairs due to the decay of a V^0 into oppositely charged particles at a vertex removed from the primary vertex. The applied restriction is a function of the p_T to counteract the tendency of large p_T to cause small values of $|d|$.

- It is required that $|\cos\theta^\star| < 0.95$, where $\theta^\star$ is the angle in the transverse plane between the vector linking the primary and secondary vertices and the charged track direction in the rest frame of the track pair.

A set of potential Λ decays is defined from the sample of V^0 candidates by demanding that:

- Track pairs are not K^0_S decay candidates. That is, it is required that the invariant mass of the track pair, $m_{\pi\pi}$, satisfy $m_{\pi\pi} < 0.45\,\mathrm{GeV/c^2}$, assuming both tracks are due to pions.

- Track pairs do not result from photon conversions. That is, the mass of the track pair m_{ee}, assuming these to be electron and positron, is such that $m_{ee} > 0.05\,\mathrm{GeV/c^2}$.

- The distance of closest approach of the tracks making up the pair is required to satisfy $|\Delta d| > 0.5\,\mathrm{cm}$.

The invariant mass spectra of the track pairs for the above samples are shown in figure 2. These are calculated assuming that both tracks are due to pions for the K^0_S candidates and for the Λ candidates that the higher momentum track is due to a proton, that with lower momentum to a pion. The final step in the selection of K^0_S candidates is the requirement that the invariant mass of the track pair, $m_{\pi\pi}$, satisfy $0.45 < m_{\pi\pi} < 0.55\,\mathrm{GeV/c^2}$. The Λ candidates are selected by requiring that $m_{p\pi}$ satisfy $1.1066 < m_{p\pi} < 1.1246\,\mathrm{GeV/c^2}$. The numbers of K^0_S and Λ candidates are 1 813 and 395 respectively.

The masses of the K^0_S and Λ are extracted from the spectra shown in figure 2 by fitting a Gaussian to the obvious peaks, using various functional forms to describe the remaining background. The backgrounds to the K^0_S and Λ signals are $8 \pm 3\%$ and $29 \pm 7\%$ respectively. The resulting masses are $m_{K^0_S} = 497.9 \pm 0.2 \pm 0.2\,\mathrm{MeV/c^2}$ and $m_\Lambda = 1115.6 \pm 0.4 \pm 0.2\,\mathrm{MeV/c^2}$, where the first error is statistical and the second systematic. The systematic error reflects the effects of varying the assumptions on the functional form of the background remaining under the signal and of residual uncertainties in the calibration of the tracking system. These values are in agreement with the current world averages quoted by the Particle Data Group (PDG) [46], namely $m^{PDG}_{K^0} = 497.672 \pm 0.031\,\mathrm{MeV/c^2}$ and $m^{PDG}_\Lambda = 1115.683 \pm 0.006\,\mathrm{MeV/c^2}$.

The numbers of K^0_S mesons and Λ baryons after background subtraction are $1\,655 \pm 41$ and 237 ± 30 respectively. There are 116 ± 21 Λ baryons and 126 ± 20 $\overline{\Lambda}$ anti-baryons. These latter

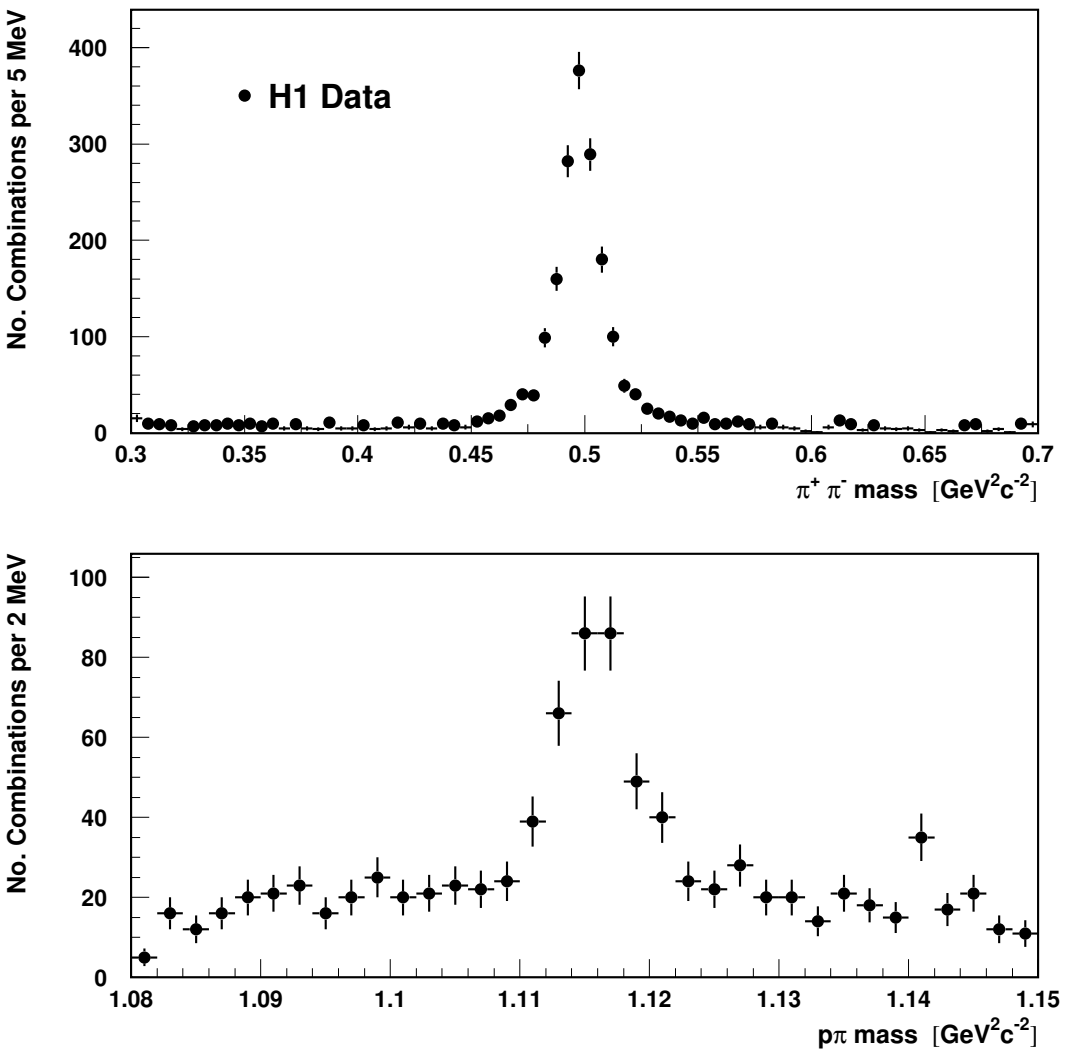

Figure 2: Pion-pion (upper graph) and proton-pion (lower graph) mass spectra for V^0 candidates in the kinematic region $10 < Q^2 < 70\,\mathrm{GeV}^2$, $10^{-4} < x < 10^{-2}$ and $0.05 < y < 0.6$ following the selection procedure described in the text.

numbers do not sum to give the total Λ plus $\overline{\Lambda}$ yield above as they are obtained from independent fits with independent background subtractions.

The detection efficiencies for K^0_S mesons and Λ baryons in the given p^2_T and η ranges are determined using Monte Carlo techniques. The efficiency for K^0_S detection is 25% at a p^2_T of $0.25\,(\mathrm{GeV/c})^2$ and rises to 40% for a p^2_T of $1\,(\mathrm{GeV/c})^2$ and above. The detection efficiency is independent of pseudo-rapidity over the measured range. The Λ detection efficiency is 12% for all η and p^2_T. There is no significant difference between the Λ and $\overline{\Lambda}$ detection efficiencies. Neither the K^0_S nor the Λ detection efficiencies depend significantly on x or Q^2.

The K^0_S and Λ lifetimes obtained using the above event samples are $\tau_{K^0_S} = 87.7 \pm 7.0 \pm 4.5$ ps and $\tau_\Lambda = 330 \pm 130 \pm 30$ ps respectively. The lifetimes are determined from the proper decay length distributions after subtracting the backgrounds extracted using the mass spectra. These are largest at small decay lengths. A correction is also applied for the decrease in K^0 and Λ detection efficiency which occurs at small decay lengths. This is determined using the LEPTO Monte Carlo with default JETSET parameters. The systematic error reflects the uncertainties in the background subtraction mentioned above and in the correction applied. The latter are estimated using half the spread of results obtained when the correction is derived using the LEPTO and CDM Monte Carlo programs with default JETSET parameters, with an additional contribution to cover the effects of deficiencies in the simulation of the H1 apparatus. The good agreement of the above results with the PDG world averages, $\tau^{PDG}_{K^0_S} = 89.26 \pm 0.12$ ps and $\tau^{PDG}_\Lambda = 263.2 \pm 2.0$ ps, confirms that the background subtraction and correction procedures are well understood.

6 Results

The observed numbers of K^0_S mesons and Λ baryons, after correction for event selection efficiency, particle detection efficiencies and branching ratios into the observed decay channels, correspond to the production of $n_{K^0} = 16\,414 \pm 403 \pm 709$ K^0 mesons and $n_\Lambda = 2\,879 \pm 373 \pm 341$ Λ baryons in the pseudo-rapidity and transverse momentum range defined by $-1.3 < \eta < 1.3$ and $0.25 < p^2_T < 4.5\,(\mathrm{GeV/c})^2$ and in the kinematic region $10 < Q^2 < 70\,\mathrm{GeV}^2$, $10^{-4} < x < 10^{-2}$ and $0.05 < y < 0.6$. The corrections are calculated by comparing the numbers of K^0 mesons and Λ baryons in events generated using the LEPTO Monte Carlo with default JETSET parameters with the numbers found after a Monte Carlo simulation of the effects of the H1 detector, reconstruction of the Monte Carlo data using the same programs as used for the H1 data, and application of the selection criteria described above. The systematic errors represent half the spread in the determination of the correction factors arising from the use of the LEPTO and CDM generators with default JETSET parameters, the aforementioned uncertainties in the parameterisation of the background mass spectra in the K^0_S and Λ mass regions, residual uncertainties in the calibration of the tracking system and deficiencies in the simulation of the H1 apparatus in the Monte Carlo program used. The effect of hard initial state photon radiation on these numbers, studied using DJANGO, is less than 2%. Hence no correction is applied, rather a contribution is added to the systematic error to cover the slight uncertainties introduced by neglecting this effect.

Monte Carlo simulations indicate that the above numbers correspond to about 20% of the total number of K^0 mesons and the same proportion of all Λ baryons produced in the x and Q^2 region studied. The systematic uncertainties associated with the extrapolation from the

measured η and p_T^2 region to all η and p_T^2 are large. Hence results quoted in this section are for the restricted region in which accurate measurement is possible.

For the reasons discussed in the introduction, it is of interest to study the K^0 and Λ spectra in η and p_T^2. The BFKL mechanism may cause excess strangeness production at large values of η and p_T^2, whereas instanton induced events contain an excess of strange particles in the range $0 \lesssim \eta \lesssim 3$. The relevant measured spectra for K^0 production in NDDIS, in the kinematic region defined above, are shown in figure 3. This figure has been corrected for acceptance

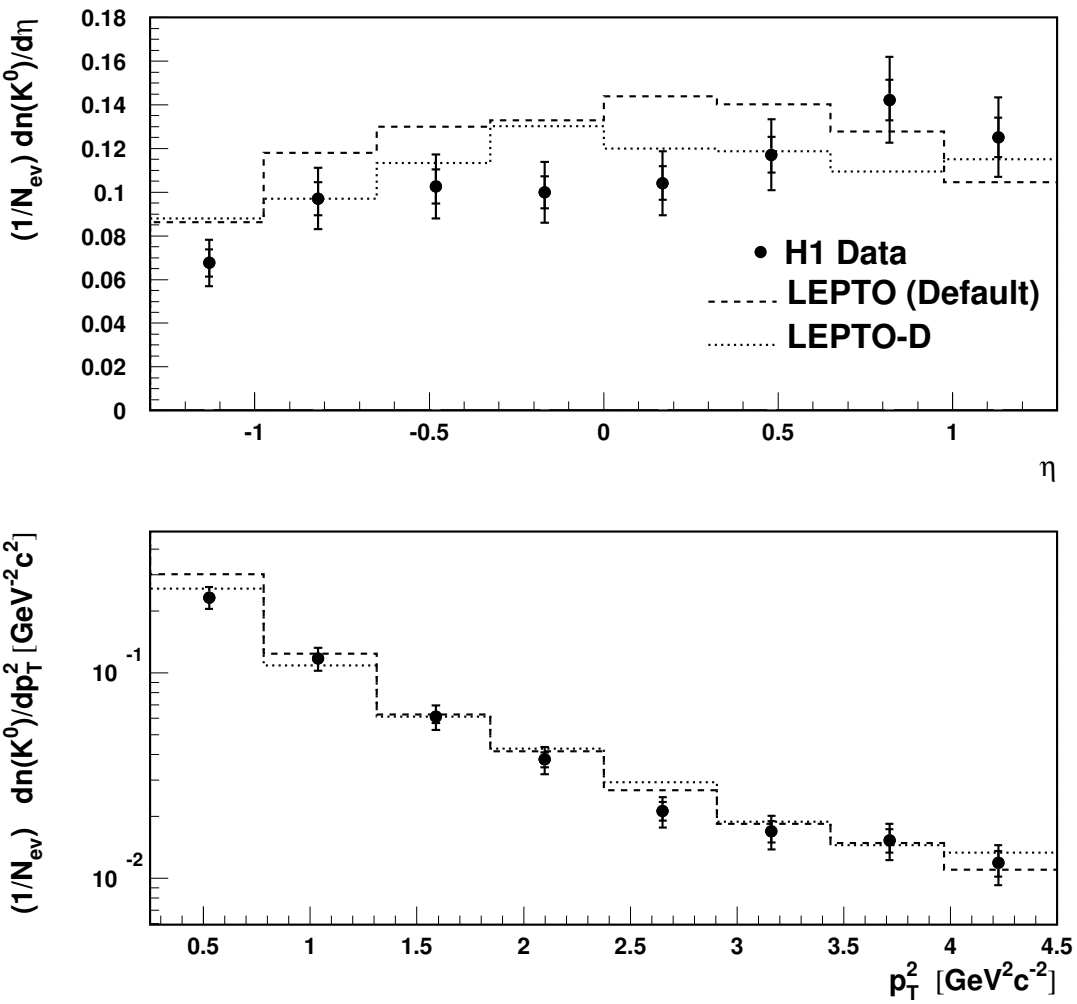

Figure 3: Measured η spectrum (upper graph) for K^0 production in the range $0.25 < p_T^2 < 4.5\,(\mathrm{GeV/c})^2$ and p_T^2 spectrum (lower graph) in the range $-1.3 < \eta < 1.3$ in non-diffractive DIS for the kinematic region $10 < Q^2 < 70\,\mathrm{GeV}^2$, $10^{-4} < x < 10^{-2}$ and $0.05 < y < 0.6$ compared with predictions from LEPTO with default JETSET parameters (LEPTO (Default)) and LEPTO with DELPHI JETSET parameters (LEPTO-D), see table 1.

and detection efficiency effects using Monte Carlo simulations, as have all subsequent figures. Here and in all following figures in which two sets of error bars are displayed the total errors are the result of adding in quadrature the statistical errors, shown using the inner error bars, and the systematic errors. The latter are estimated as previously described. Comparisons are made with the predictions of LEPTO using the default fragmentation parameters ($\lambda_s = 0.3$), and using the set of parameters extracted by the DELPHI collaboration ($\lambda_s = 0.23$, see table 1). The normalisation of the Monte Carlo predictions is to the corrected number of NDDIS events in the specified x and Q^2 range. In this and in other distributions it is observed that the description of the data provided using the DELPHI JETSET parameters in the LEPTO and CDM Monte Carlo models is significantly better than that obtained with the default settings. The parameter change that has the largest effect on the Monte Carlo predictions discussed here is the modification to λ_s. A similar level of agreement is obtained if the strangeness suppression factor favoured by E665 ($\lambda_s = 0.2$) is used. Once the modification to the fragmentation parameters has been made the description of the data is reasonable. There is no evidence for anomalous strangeness production in either the absolute normalisation or the shape of the measured distributions.

The above agreement of the Monte Carlo predictions for the average number of K^0 mesons per event with the measurement does not prove that the distribution of the number of K^0 mesons per event is correctly described. The models might produce a larger number of strange particles in a smaller proportion of the events than observed in the data, or vice-versa. However, this is not the case, as may be seen from the following observation. The corrected proportion of NDDIS events containing two kaons in the kinematic region studied is $0.044 \pm 0.009 \pm 0.012$. This number is to be compared with the LEPTO Monte Carlo predictions of 0.065 and 0.056 with default and DELPHI JETSET parameters respectively, and with the corresponding CDM predictions of 0.060 and 0.044. HERWIG predicts that the proportion of di-kaon events is 0.059. Agreement with the Monte Carlo models which use JETSET is again observed to be better if the lower λ_s value is used. There is no evidence for anomalous production of events containing many kaons.

The Λ spectra in η and p_T^2 are shown in figure 4. The statistical precision of these data does not allow discrimination between the default and DELPHI sets of JETSET parameters. The broad agreement with the Monte Carlo predictions indicates that the mechanisms responsible for di-quark production in the fragmentation in DIS at low x are similar to those at work in other processes and at higher values of x.

In order to allow some separation between strangeness produced in the hard scattering and in the softer fragmentation process, K^0 production is also studied as a function of the fragmentation variable z, defined as

$$z = \frac{E_{K^0} + p_{L,K^0}}{2E_q},$$

where E_{K^0} and p_{L,K^0} are the energy of the K^0 and the component of its momentum along the struck quark direction, given by the four-momentum $q + xp$. This may be calculated using the measured parameters of the scattered positron and is the direction expected for the scattered quark in the naïve Quark Parton Model. The quantity E_q is the energy expected for the struck quark, assumed massless, using the same approximation. Strange quarks may be produced in the hard scattering either through the interaction of the virtual boson with a strange sea quark, or directly via the BGF process, or through the decay of c quarks produced via BGF. The K^0 mesons formed from strange quarks produced by these means, referred to as "hard K^0s", are likely to be at larger z than those produced in the fragmentation chain following, say, the

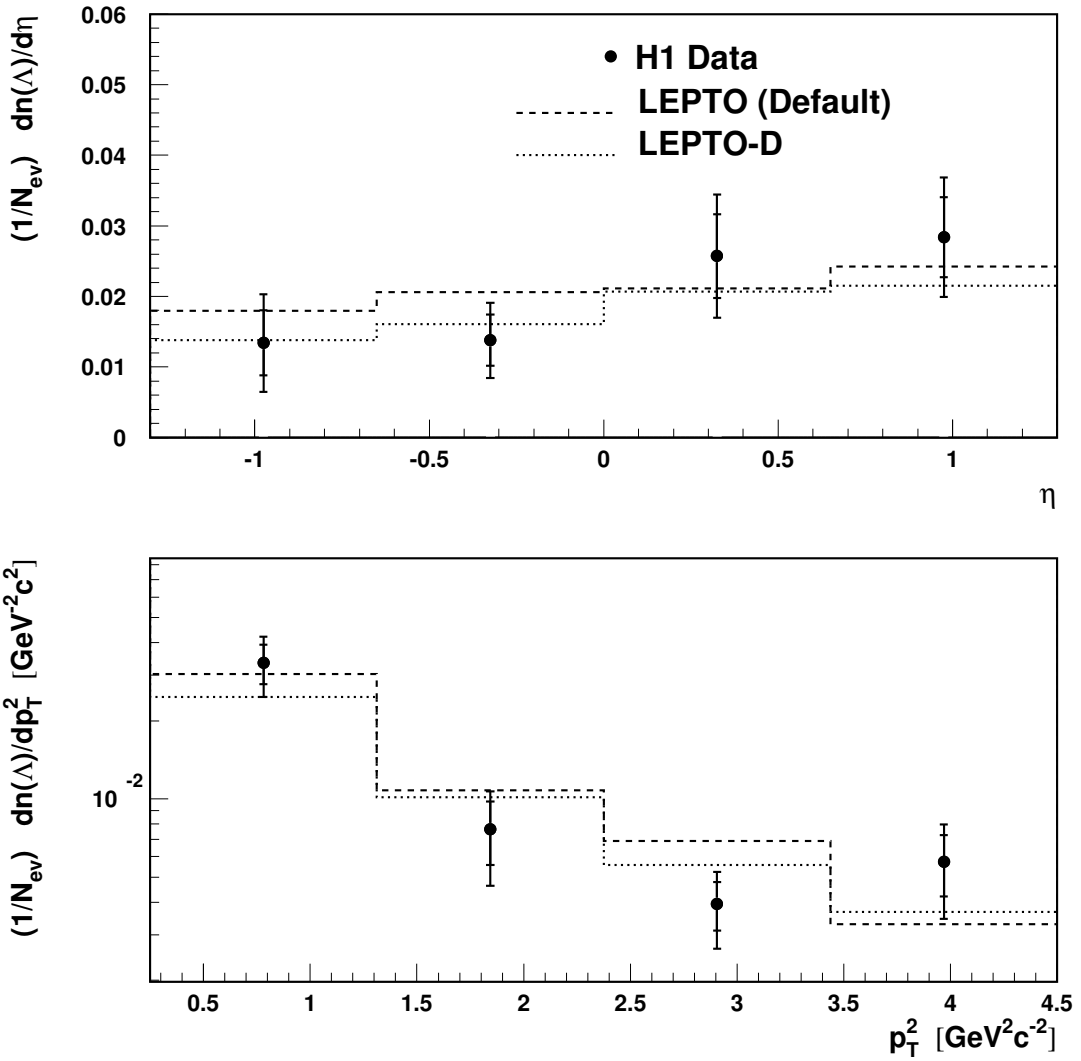

Figure 4: Measured η spectrum (upper graph) for Λ production in the range $0.25 < p_T^2 < 4.5\,(\mathrm{GeV/c})^2$ and p_T^2 spectrum (lower graph) in the range $-1.3 < \eta < 1.3$ in non-diffractive DIS for the kinematic region $10 < Q^2 < 70\,\mathrm{GeV}^2$, $10^{-4} < x < 10^{-2}$ and $0.05 < y < 0.6$ compared with predictions from LEPTO with default JETSET parameters (LEPTO (Default)) and LEPTO with DELPHI JETSET parameters (LEPTO-D), see table 1.

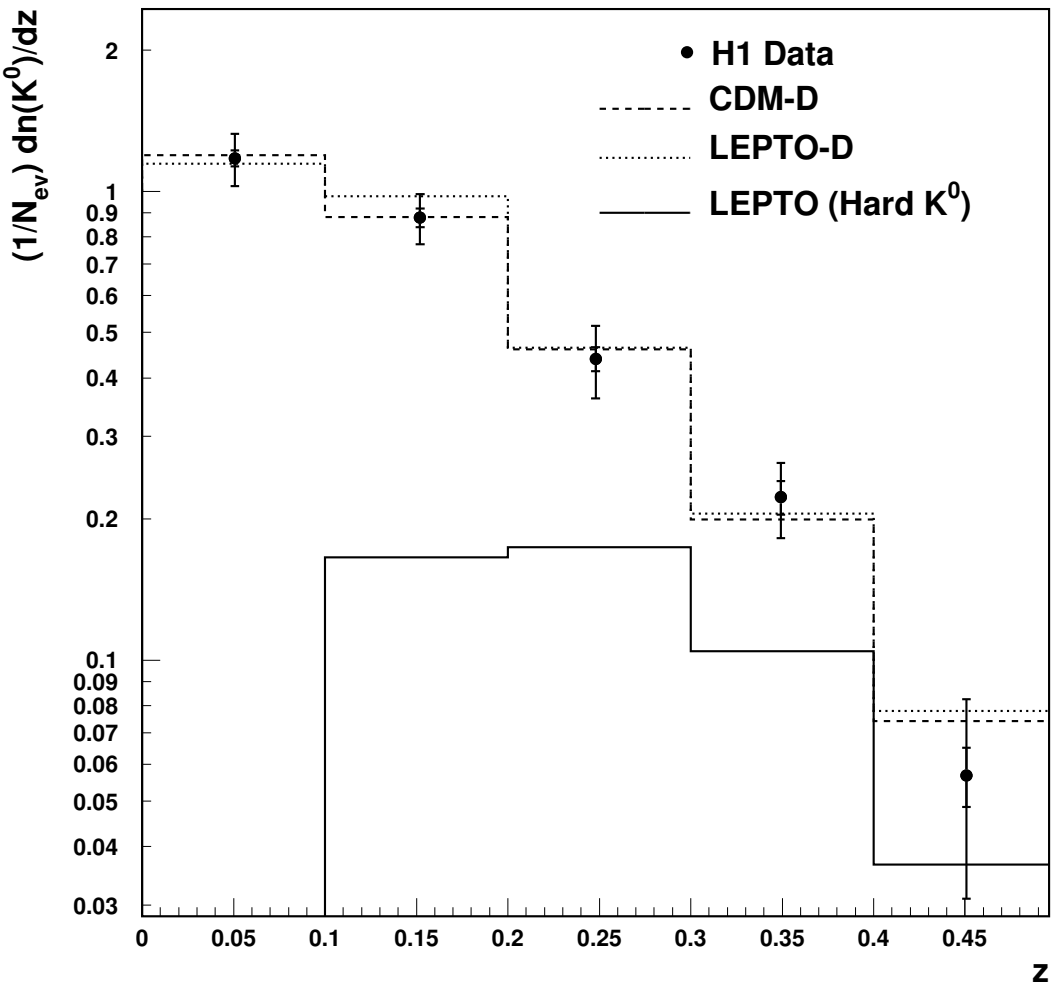

Figure 5: Measured z spectrum for K^0 production in the range $0.25 < p_T^2 < 4.5\,(\mathrm{GeV/c})^2$ and $-1.3 < \eta < 1.3$ in non-diffractive DIS for the kinematic region $10 < Q^2 < 70\,\mathrm{GeV}^2$, $10^{-4} < x < 10^{-2}$ and $0.05 < y < 0.6$ compared with predictions from LEPTO with DELPHI JETSET parameters (LEPTO-D) and the CDM with DELPHI JETSET parameters (CDM-D), see table 1; also shown is the spectrum obtained from LEPTO if only K^0 mesons which contain a strange quark produced in the hard interaction are considered (LEPTO (Hard K^0)).

interaction of the virtual photon with a u quark. Hence anomalous K^0 production at large z is likely to be associated with the hard sub-process, that at smaller z with the hadronisation. The K^0 spectrum in z is shown in figure 5. The Monte Carlo curves displayed in this figure are obtained using LEPTO and the CDM. Of interest is the curve obtained when only hard K^0 mesons are considered. These are found to populate the high z region of the distribution, as expected, and form about 20% of the total number of K^0 mesons produced by the LEPTO

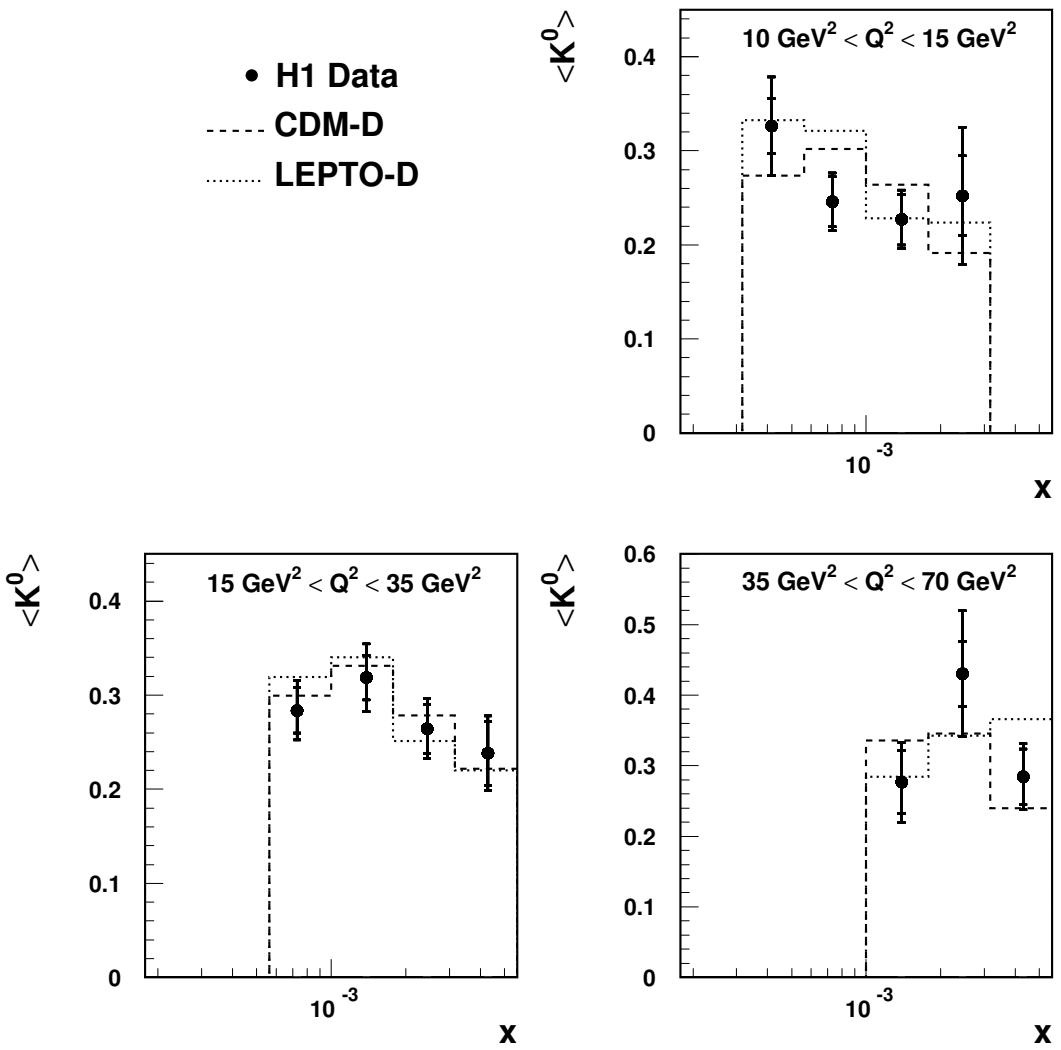

Figure 6: Mean numbers of K^0 mesons per NDDIS event produced in the range $0.25 < p_T^2 < 4.5\,(\mathrm{GeV/c})^2$ and $-1.3 < \eta < 1.3$ as a function of x, with the restriction $0.05 < y < 0.6$, in non-diffractive DIS in the Q^2 regions indicated compared with predictions from LEPTO with DELPHI JETSET parameters (LEPTO-D) and the CDM with DELPHI JETSET parameters (CDM-D), see table 1.

generator in the kinematic region studied when using the DELPHI JETSET parameters. About 40% of these result from c quark decays. There is no evidence for anomalous production of strangeness associated with either the high or low z regions of the distribution.

In figure 6 are shown the mean numbers of K^0 mesons observed per NDDIS event as a function of x in the Q^2 regions $10 < Q^2 < 15\,\mathrm{GeV}^2$, $15 < Q^2 < 35\,\mathrm{GeV}^2$ and $35 < Q^2 < 70\,\mathrm{GeV}^2$. There is no evidence for any systematic deviation as a function of either Q^2 or x between the Monte Carlo predictions shown here and the data. As stated in the introduction, BFKL

dynamics may cause additional K^0 production at large values of η and at small x. It has been argued that the CDM gluon radiation prescription models to some extent the effects of BFKL evolution on the hadronic state [47]. The similarity of the LEPTO and CDM predictions in figure 6 would then indicate that, in the η region studied, there is no sensitivity to any putative additional strangeness production due to BFKL dynamics. A definitive statement must await a Monte Carlo implementation of the BFKL evolution prescription.

An alternative way of examining the K^0 production data is to consider the ratio of the number of K^0 mesons produced to the number of primary charged tracks. This latter is defined to be the number of primary charged tracks in the transverse momentum and pseudo-rapidity region given by $p_T > 0.15\,\mathrm{GeV/c}$, $-1.3 < \eta < 1.3$ and is corrected for detection efficiencies using Monte Carlo simulations. This means of presenting the data maintains sensitivity to effects that change the ratio of strange to non-strange quark production while reducing the effect of global multiplicity changes. Hence, for example, shifts in the strangeness suppression factor may be observed with reduced sensitivity to hadronisation variables which tend to change the overall track multiplicity. The production ratios, in the Q^2 regions defined above, are shown in figure 7. Again, better agreement with Monte Carlo simulations is observed when using the DELPHI than when using the default JETSET parameters, providing further evidence that it is indeed the suppression of strangeness production in the hadronisation that is responsible for the differences, rather than a global discrepancy in the modelling of the multiplicity.

Comparisons of the K^0 spectra in η and p_T^2 for DDIS events with calculations using RAPGAP are shown in figure 8. These data are corrected to the range $x_{I\!P} < 0.05$ and to the x and Q^2 region defined above using the results of the RAPGAP-PS Monte Carlo and a full simulation of the effects of H1 detector. The RAPGAP-CDM predictions, made with the default JETSET parameters, are seen to lie a little above the measurements, as is the case for NDDIS. The agreement with RAPGAP-PS is somewhat better.

The total rates of strange particle production in both DDIS and NDDIS are listed in table 2. They reveal that the level of strangeness production in DDIS is somewhat lower than that in NDDIS. This effect is probably due to the decreased overall level of particle production in DDIS in the η region studied, a consequence of the lower hadronic mass of the fragmenting system ($M_X < W$), rather than a difference in the strangeness suppression factor. This argument is supported by the observation that the ratio of K^0 mesons to all charged particles in DDIS is consistent with that in NDDIS. Given that the overwhelming contribution to proton structure in the x range studied here is made by gluons, this observation is consistent with the electron-gluon scattering picture of DDIS. The consistency with the picture in which the scattering occurs between the positron and a flavour singlet pomeron is demonstrated by the agreement observed between the RAPGAP predictions and the DDIS measurements of the K^0 to charged track ratio.

It is also apparent from table 2 that the difference in the two RAPGAP DDIS calculations of the K^0 multiplicity largely disappears when the ratio of that multiplicity to the primary charged particle multiplicity is considered. This occurs as the RAPGAP-CDM generator tends to produce a higher charged particle multiplicity than that seen with RAPGAP-PS.

7 Comparison with Previous Measurements

Figure 9 shows the η spectra for K^0 and Λ production in DIS (NDDIS and DDIS) after correction

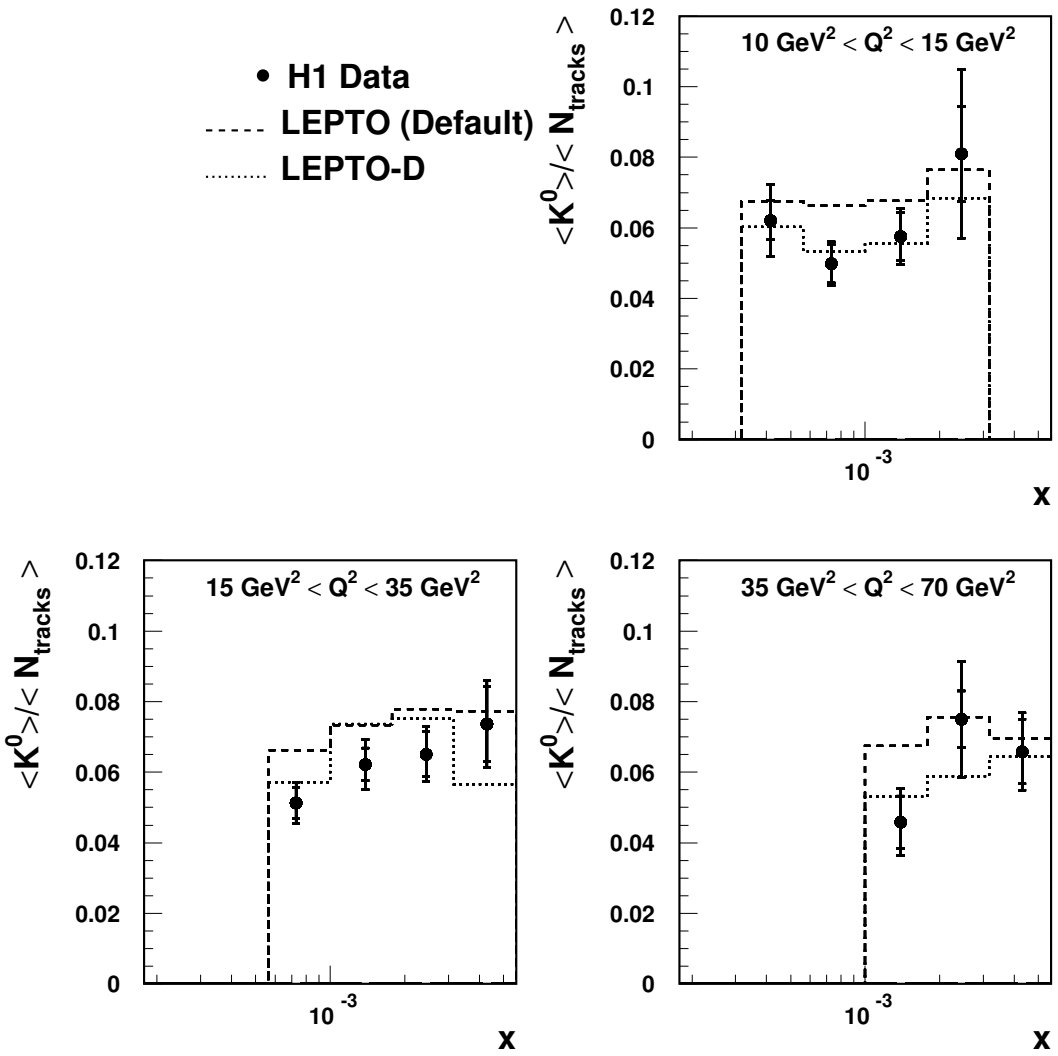

Figure 7: Measured ratios of the number of K^0 mesons in the range $0.25 < p_T^2 < 4.5\,(\mathrm{GeV/c})^2$ and $-1.3 < \eta < 1.3$ to all primary charged tracks with $p_T > 0.15\,\mathrm{GeV/c}$ as a function of x, with the restriction $0.05 < y < 0.6$ in non-diffractive DIS in the Q^2 regions indicated compared with predictions from LEPTO with default JETSET parameters (LEPTO(Default)) and LEPTO with DELPHI JETSET parameters (LEPTO-D), see table 1.

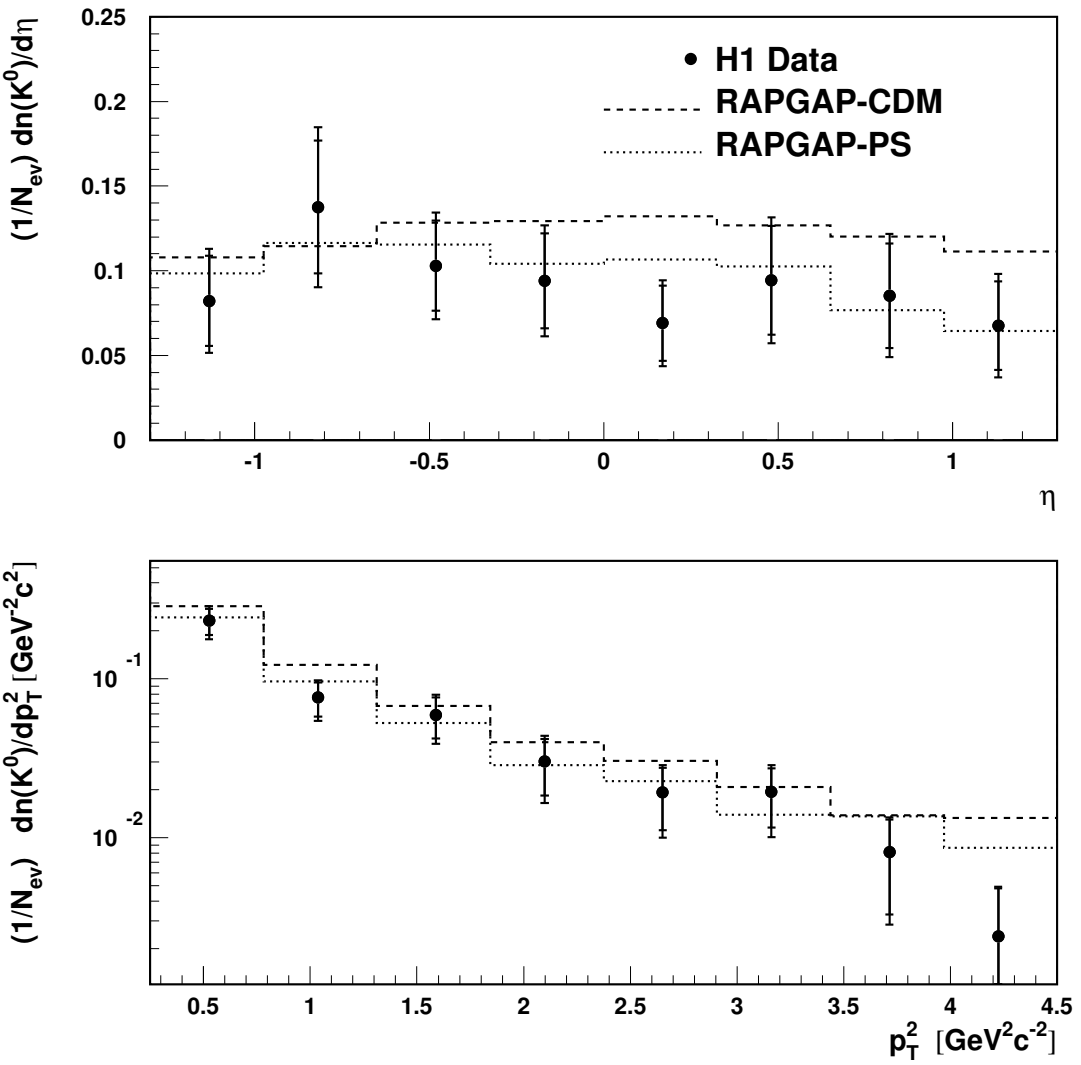

Figure 8: Measured η spectrum (upper graph) for K^0 production in the range $0.25 < p_T^2 < 4.5\,(\mathrm{GeV/c})^2$ and p_T^2 spectrum (lower graph) in the range $-1.3 < \eta < 1.3$ in diffractive DIS for the kinematic region $10 < Q^2 < 70\,\mathrm{GeV}^2$, $10^{-4} < x < 10^{-2}$, $0.05 < y < 0.6$ and $x_{I\!P} < 0.05$ compared with predictions from RAPGAP-PS and RAPGAP-CDM.

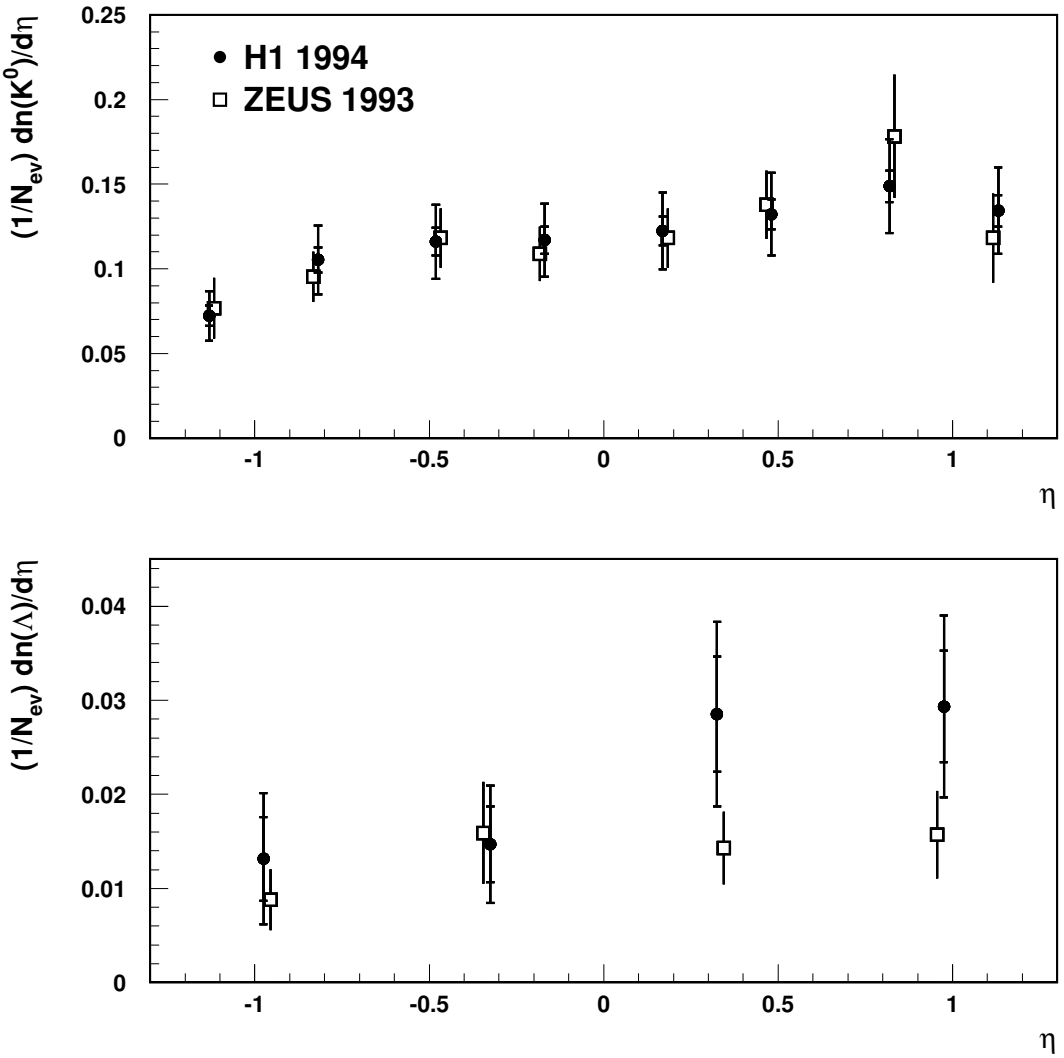

Figure 9: Measured η spectrum for K^0 production (upper graph) and for Λ production (lower graph) in the kinematic region $10 < Q^2 < 640\,\mathrm{GeV}^2$, $0.0003 < x < 0.01$ and $y > 0.04$; the K^0 results are for the range $0.5 < p_T < 4.0\,\mathrm{GeV/c}$ and the Λ results for $0.5 < p_T < 3.5\,\mathrm{GeV/c}$, compared with the measurements of the ZEUS collaboration made in deep-inelastic electron-proton scattering at HERA.

Data-Set	No. K^0/event	No. Λ/event	No. K^0/No. tracks
H1 NDDIS data	0.278±0.008±0.012	0.053±0.007±0.007	0.058±0.002±0.003
CDM (default)	0.316	0.052	0.066
CDM (DELPHI)	0.284	0.047	0.062
CDM (E665)	0.260	0.042	0.054
LEPTO (default)	0.320	0.055	0.068
LEPTO (DELPHI)	0.282	0.047	0.064
LEPTO (E665)	0.267	0.040	0.056
HERWIG	0.316	0.047	0.068
H1 DDIS data	0.238±0.026±0.016	0.026±0.010±0.025	0.063±0.007±0.004
RAPGAP-PS	0.255	0.032	0.072
RAPGAP-CDM	0.316	0.040	0.074

Table 2: Measured mean K^0 and Λ multiplicities with $0.25 < p_T^2 < 4.5\,(\mathrm{GeV/c})^2$ and $-1.3 < \eta < 1.3$ for the kinematic region $10 < Q^2 < 70\,\mathrm{GeV}^2$, $10^{-4} < x < 10^{-2}$ and $0.05 < y < 0.6$ and the ratio of the above multiplicities to the mean multiplicity of primary charged particles with $p_T > 0.15\,\mathrm{GeV/c}$ in the same kinematic region in diffractive and non-diffractive DIS together with the predictions of various Monte Carlo models.

to the transverse momentum range $0.5 < p_T < 4.0\,\mathrm{GeV/c}$ in the case of the K^0 mesons and $0.5 < p_T < 3.5\,\mathrm{GeV/c}$ for the Λ baryons and the kinematic region $10 < Q^2 < 640\,\mathrm{GeV}^2$, $0.0003 < x < 0.04$ and $y > 0.04$. The correction is performed using the LEPTO Monte Carlo with DELPHI JETSET parameters. The systematic errors shown include contributions due to the uncertainties in the correction procedure estimated using the spread of results obtained when the default JETSET parameters are used with LEPTO and both the default and DELPHI JETSET parameters with the CDM. Although the central values obtained are very similar to those shown in figures 3 and 4, the correction is to a kinematic region which includes a significant range outside the reach of the current measurement and hence the associated systematic errors are larger than those shown in figures 3 and 4. These results are directly comparable with the measurements of the ZEUS collaboration [7], also shown in figure 9, obtained in deep-inelastic electron-proton scattering at HERA. The two sets of data are seen to be in reasonable agreement.

In order to facilitate comparison with other measurements, in the remainder of this section the K^0 and Λ NDDIS production results are presented as functions of various quantities in the hadronic centre-of-mass frame with the z direction chosen to be that of the exchanged virtual boson. The transformation to this frame is made using the measured energy and angle of the scattered electron.

Figure 10 shows the K^0 production rate as a function of Feynman-x, the fractional longitudinal centre-of-mass momentum $x_F = 2p_L^*/W$. The data are also given in table 3. The x_F range shown is restricted to the region in which, for the laboratory pseudo-rapidity and transverse momentum region over which particle identification is possible, the acceptance is at least 20%, namely $0.05 < x_F < 0.40$. The average acceptance over this range is 35%. The resulting mean centre-of-mass energy is $\langle W \rangle = 138\,\mathrm{GeV}$. The measurements are corrected for the detector acceptance, the region of laboratory pseudo-rapidity and transverse momentum in which particle identification is performed, and the kinematic region studied. The correction is performed using the LEPTO Monte Carlo with DELPHI JETSET parameters. The systematic errors represent

x_F	$\frac{1}{N}\frac{dn}{dx_F}$
$0.05 - 0.10$	$3.06 \pm 0.23 \pm 0.83$
$0.10 - 0.15$	$1.60 \pm 0.14 \pm 0.19$
$0.15 - 0.20$	$1.07 \pm 0.11 \pm 0.15$
$0.20 - 0.25$	$0.68 \pm 0.09 \pm 0.12$
$0.25 - 0.30$	$0.48 \pm 0.08 \pm 0.16$
$0.30 - 0.40$	$0.28 \pm 0.05 \pm 0.07$

Table 3: The K^0 spectrum as a function of Feynman-x (x_F) at $\langle W \rangle = 138\,\mathrm{GeV}$ for the range $10 < Q^2 < 70\,\mathrm{GeV}^2$ (see figure 10).

the dispersion arising from using the default JETSET parameters with LEPTO and both the default and DELPHI JETSET parameters with the CDM in the correction procedure and the effects of the accuracy with which the transformation to the centre-of-mass frame can be performed. The shifts resulting from initial state photon radiation, studied using DJANGO, are found to be small and hence are not corrected for. The systematic error contains a contribution covering their effects. Both the CDM and LEPTO Monte Carlo models describe the x_F spectrum well, provided the DELPHI JETSET parameters are used. The agreement with the HERWIG Monte Carlo is also good.

Also shown in figure 10 are the data of the EMC collaboration [48], obtained in muon-proton scattering at $\sqrt{\langle W^2 \rangle} = 11.4\,\mathrm{GeV}$, and of the E665 collaboration [6], obtained in muon-nucleon scattering at $\langle W \rangle = 17.1\,\mathrm{GeV}$. These lie below the H1 data and fall less steeply with x_F, the differences being more pronounced for the lower energy EMC data[1]. This observation may be largely explained by the extra phase space available for QCD radiation at the higher centre-of-mass energy available at HERA.

Comparisons of the x_F spectra with electron-positron data are complicated by the direct production of heavy quarks in electron-positron annihilation, with subsequent decay to strange quarks and hence enhanced strange particle production. This problem is partially solved here by making the comparison with Monte Carlo predictions for electron-positron annihilation to u, d and s quarks only, at the H1 centre-of-mass energy. Residual differences are to be expected as the proportion of primary s quarks produced in the simulation is still not the same as that in DIS at this energy. The Monte Carlo used (JETSET with DELPHI tuning) accurately describes electron-positron annihilation data when the production of all possible flavours is allowed [11]. A further complication is that the electron-positron annihilation data are available in terms of the fractional centre-of-mass momentum, $x_p = 2p/W$. However, the transverse momenta in the hadronic centre-of-mass frame, p_T^*, of the K^0 mesons studied here are generally much smaller than their longitudinal momenta and so the momentum $p \approx p_L$. Hence $x_F = x_p$ to an accuracy better than that represented by the symbol size in the figures. The K^0 spectrum in x_p from the JETSET simulation, divided by two to compensate for the production of a quark anti-quark pair in electron-positron annihilation, may thus be expected to be similar to the x_F spectrum resulting from the struck quark in NDDIS. That this is the case is seen in figure 10.

Despite their lower precision, the Λ measurements, shown in table 4 and figure 11, reveal a

[1] Note that the EMC data here are at a lower centre-of-mass energy than those compared with H1 results in [49].

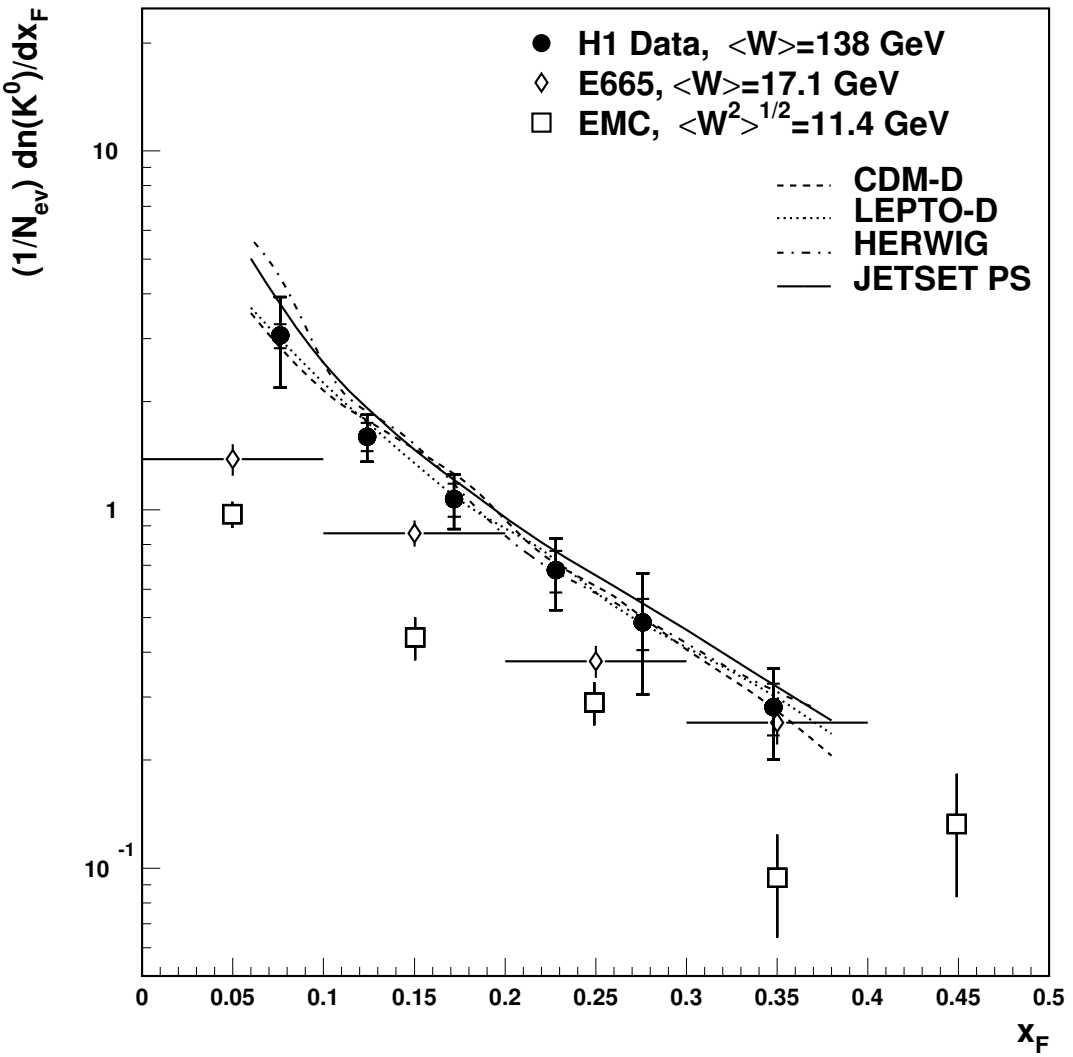

Figure 10: Production of K^0 mesons as a function of Feynman-x (x_F) in the range $10 < Q^2 < 70\,\mathrm{GeV}^2$ compared with the muon-proton and muon-nucleon scattering results of the EMC and E665 collaborations, the results of a Monte-Carlo simulation of electron-positron annihilation to u, d and s quarks at the same centre-of-mass energy as the H1 data (JETSET PS) and various other Monte Carlo simulations of DIS.

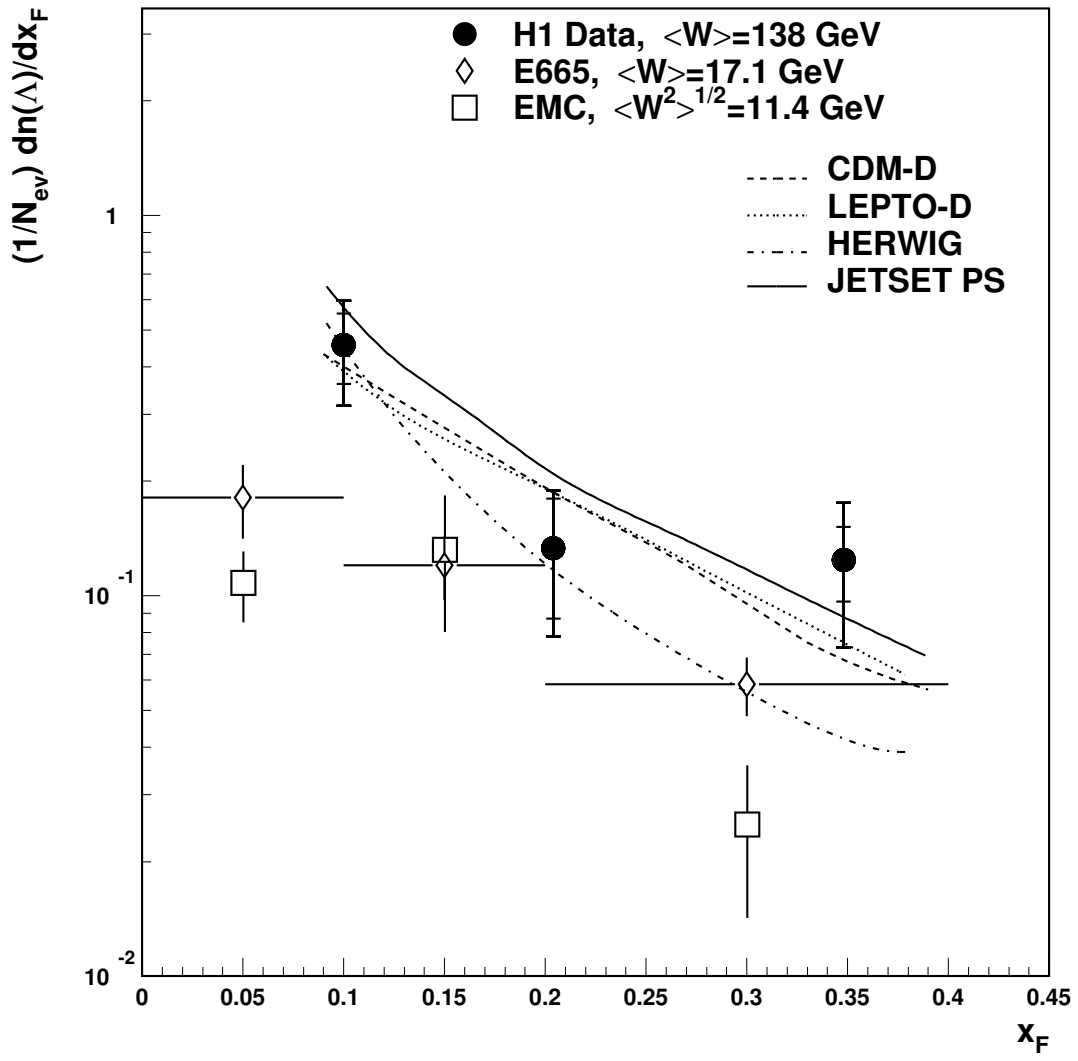

Figure 11: Production of Λ baryons as a function of Feynman-x (x_F) in the range $10 < Q^2 < 70\,\mathrm{GeV}^2$ compared with the muon-proton and muon-nucleon scattering results of the EMC and E665 collaborations, the results of a Monte-Carlo simulation of electron-positron annihilation to u, d and s quarks at the same centre-of-mass energy as the H1 data (JETSET PS) and various other Monte Carlo simulations of DIS.

x_F	$\frac{1}{N}\frac{dn}{dx_F}$
$0.05 - 0.15$	$0.46 \pm 0.10 \pm 0.10$
$0.15 - 0.25$	$0.13 \pm 0.05 \pm 0.03$
$0.25 - 0.45$	$0.12 \pm 0.03 \pm 0.04$

Table 4: The Λ spectrum as a function of Feynman-x at $\langle W \rangle = 138\,\mathrm{GeV}$ for the range $10 < Q^2 < 70\,\mathrm{GeV}^2$(see figure 11).

x_F	$\langle p_T^{*2} \rangle$
$0.05 - 0.10$	$0.47 \pm 0.06 \pm 0.09$
$0.10 - 0.15$	$0.84 \pm 0.06 \pm 0.38$
$0.15 - 0.20$	$0.85 \pm 0.09 \pm 0.27$
$0.20 - 0.40$	$1.70 \pm 0.08 \pm 0.42$

Table 5: Corrected values of K^0 $\langle p_T^{*2} \rangle$ as a function of Feynman-x at $\langle W \rangle = 117\,\mathrm{GeV}$ for the range $10 < Q^2 < 70\,\mathrm{GeV}^2$ (see figure 12).

similar trend to the K^0 results discussed above when compared with the lower energy EMC [48] and E665 [6] measurements. The agreement with the results of a simulation of electron-positron annihilation as described above is good. The HERWIG expectations differ from those of LEPTO and the CDM somewhat, but the data are not precise enough to discriminate between the models.

The relationship between the fractional longitudinal momentum and the mean squared transverse momentum, which is sensitive to QCD radiation effects, is often illustrated in the "seagull" plot. Such a plot is shown for K^0 production in figure 12, the data also being given in table 5. Here, the W range of the data is restricted in order to reduce the mean centre-of-mass energy to $\langle W \rangle = 117\,\mathrm{GeV}$, comparable with previously published H1 data on charged particle production [49], also shown in the figure. The K^0 and charged particle measurements are seen to be in good agreement and both lie at higher $\langle p_T^{*2} \rangle$ for a given x_F than the lower centre-of-mass energy measurements of the E665 and EMC collaborations. This difference is expected within the framework of QCD due to the effects of increased radiation at the higher energy. The CDM and LEPTO models, with DELPHI JETSET parameters, are able to describe the data well. HERWIG (not shown) describes the data shown here with a similar level of precision.

In order to study more directly the behaviour of K^0 and Λ production with the hadronic centre-of-mass energy, the mean K^0 and Λ multiplicities are shown as a function of W^2 in figure 13 and are also given in tables 6 and 7. These multiplicities are corrected so that they represent the numbers of particles produced with $x_F > 0$. A procedure similar to that described above is used to obtain the correction and the associated systematic error. Both the K^0 and Λ measurements show that the logarithmic increase in mean multiplicity observed at lower energies (here data are shown from the E665 collaboration and from the anti-neutrino and neutrino-proton scattering experiments of the WA21 collaboration [8]) persists to the much higher energies available at HERA.

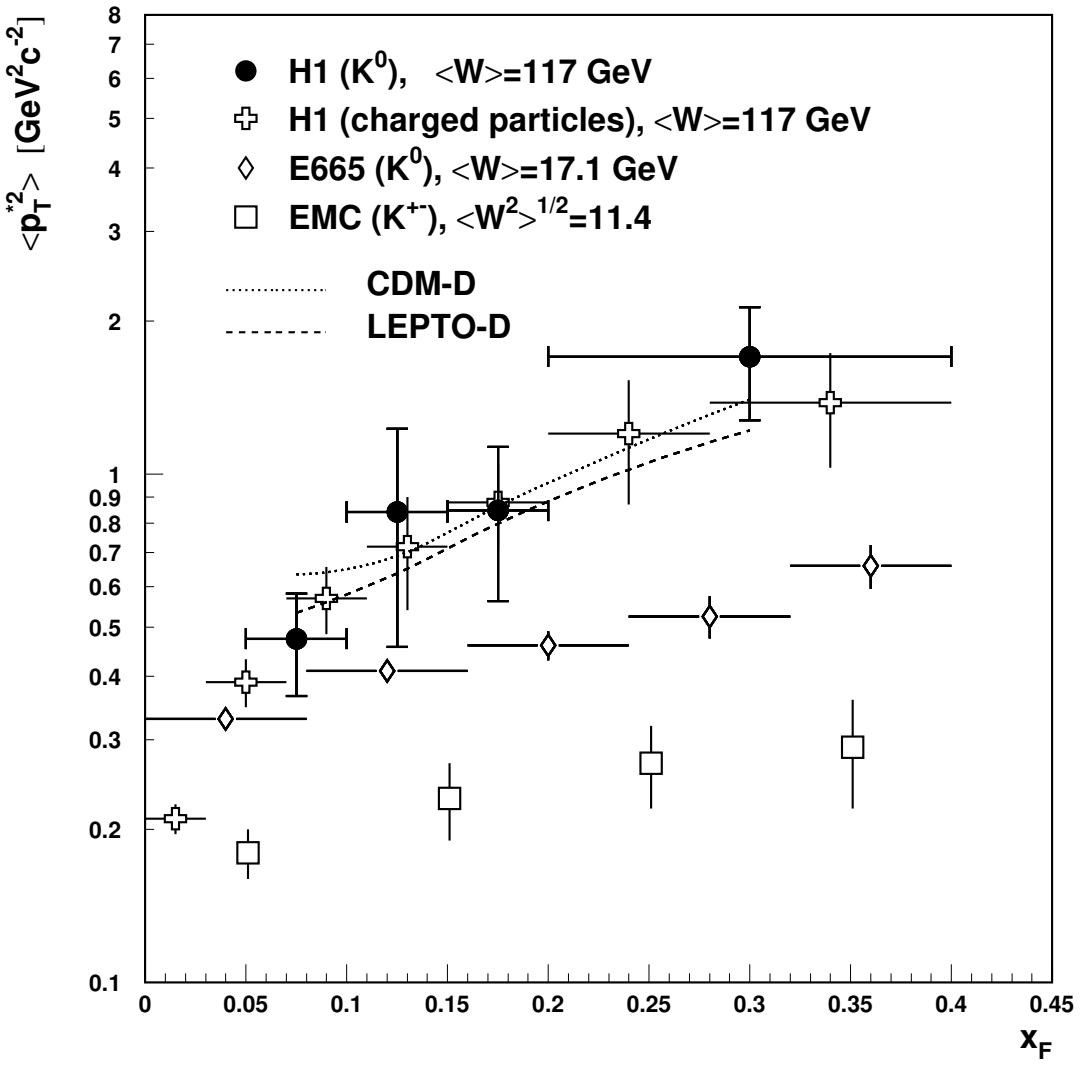

Figure 12: The mean squared transverse hadronic centre-of-mass momentum ($\langle p_T^{*2} \rangle$) of K^0 mesons and of all charged particles as a function of Feynman-x (x_F) in the range $10 < Q^2 < 70\,\mathrm{GeV}^2$ compared with measurements of K^0 and $K^{\pm}$ production in muon-nucleon and muon-proton scattering made by the E665 and EMC collaborations; also shown are various Monte Carlo predictions.

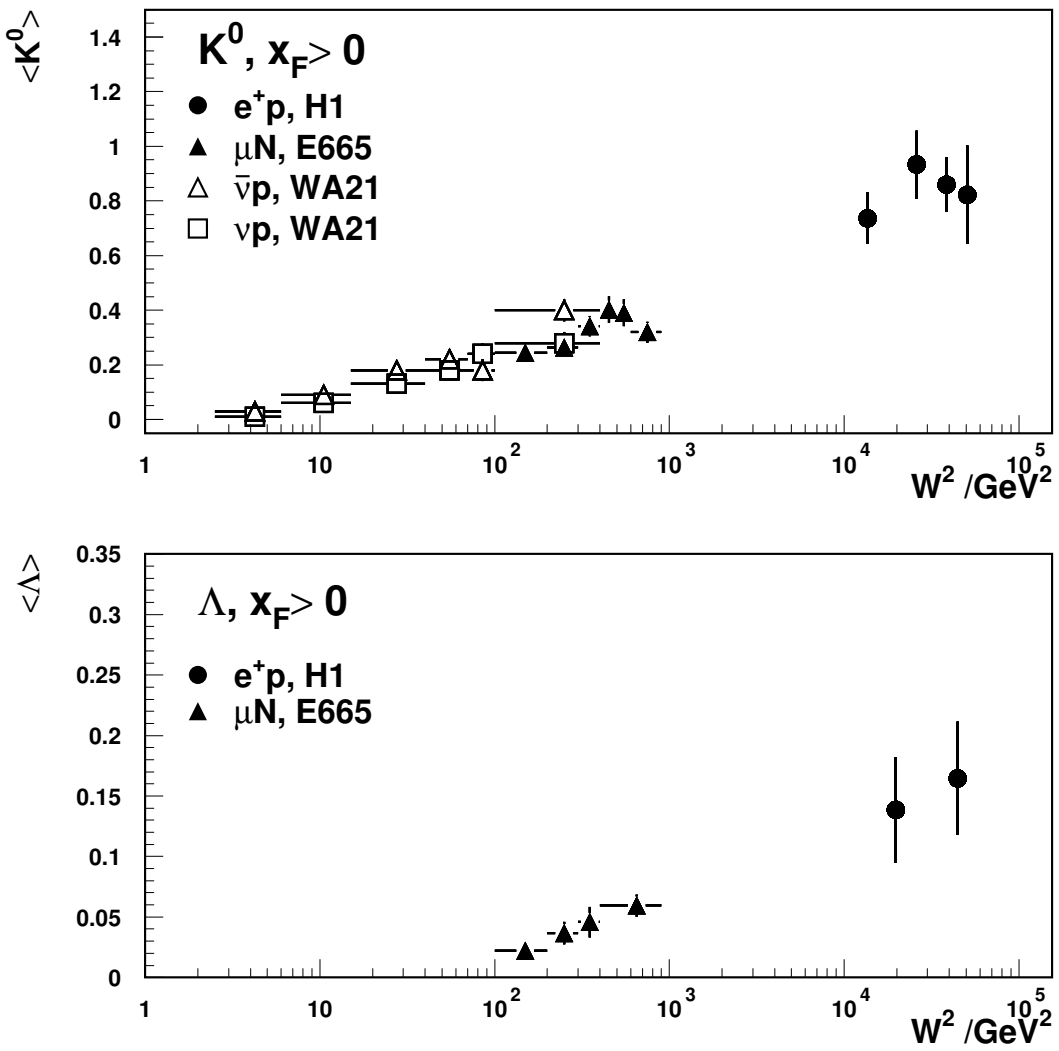

Figure 13: The mean K^0 (upper graph) and Λ (lower graph) multiplicities for $x_F > 0$ as a function of W^2 in the range $10 < Q^2 < 70\,\mathrm{GeV}^2$ compared with the muon-nucleon scattering results of the E665 collaboration and WA21 measurements from anti-neutrino and neutrino-proton scattering.

W^2 (GeV^2)	$\langle K^0 \rangle$
6400 – 19300	$0.74 \pm 0.03 \pm 0.09$
19300 – 32200	$0.93 \pm 0.05 \pm 0.11$
32200 – 45100	$0.86 \pm 0.06 \pm 0.08$
45100 – 58000	$0.82 \pm 0.09 \pm 0.16$

Table 6: Mean K^0 multiplicity for $x_F > 0$ in the hadronic centre-of-mass frame as a function of W^2 (see figure 13).

W^2 (GeV^2)	$\langle \Lambda \rangle$
6400 – 15625	$0.13 \pm 0.03 \pm 0.03$
15625 – 58000	$0.17 \pm 0.03 \pm 0.04$

Table 7: Mean Λ multiplicity for $x_F > 0$ in the hadronic centre-of-mass system as function of W^2 for the range $10 < Q^2 < 70\,\mathrm{GeV}^2$(see figure 13).

8 QCD Instanton Production

If a significant proportion of DIS events were induced by QCD instantons, large changes in the strangeness composition of the hadronic final state would be expected. This is illustrated in figure 14 where, to ensure reliable simulation using the instanton generator, the kinematic region studied is further restricted to $10 < Q^2 < 70\,\mathrm{GeV}^2$, $10^{-3} < x < 10^{-2}$ and $0.1 < y < 0.6$. The number of events in this region is 16 486 after the application of the NDDIS selection criteria. In order to determine an upper limit for the cross-section for instanton induced events it is then assumed that the measured rate of K^0 production, shown as a function of η in figure 15, is the result of a proportion f of instanton induced events with the rest being due to the NDDIS models discussed above. A χ^2 minimisation procedure is used to determine the value of f.

When using LEPTO and the CDM to calculate the rate expected for NDDIS without an instanton contribution, the DELPHI λ_s value and other fragmentation parameters are used as these are determined in electron-positron annihilation, in which there is no contribution from instanton induced events. The results obtained are $f = -0.044 \pm 0.032$ and $f = -0.002 \pm 0.031$ using QCDINS with HERWIG and the CDM respectively. The largest value of f is obtained using QCDINS with LEPTO and is $f = 0.006 \pm 0.030$. The fit to the measured K^0 production rate resulting in this latter case is shown in figure 15. The f values are consistent with being zero and hence a 95% confidence level upper limit of 0.9 nb is placed on the cross-section for instanton induced events in the above kinematic region, where the largest f value is used in the determination of the limit. The limit is of the same order of magnitude as a recent, albeit uncertain, determination of the cross-section for QCD instanton induced events in DIS [50].

9 Conclusions

Strangeness production in deep-inelastic positron-proton scattering (DIS) is studied using the H1 apparatus at the HERA collider at DESY. The rates of K^0 meson and Λ baryon production are

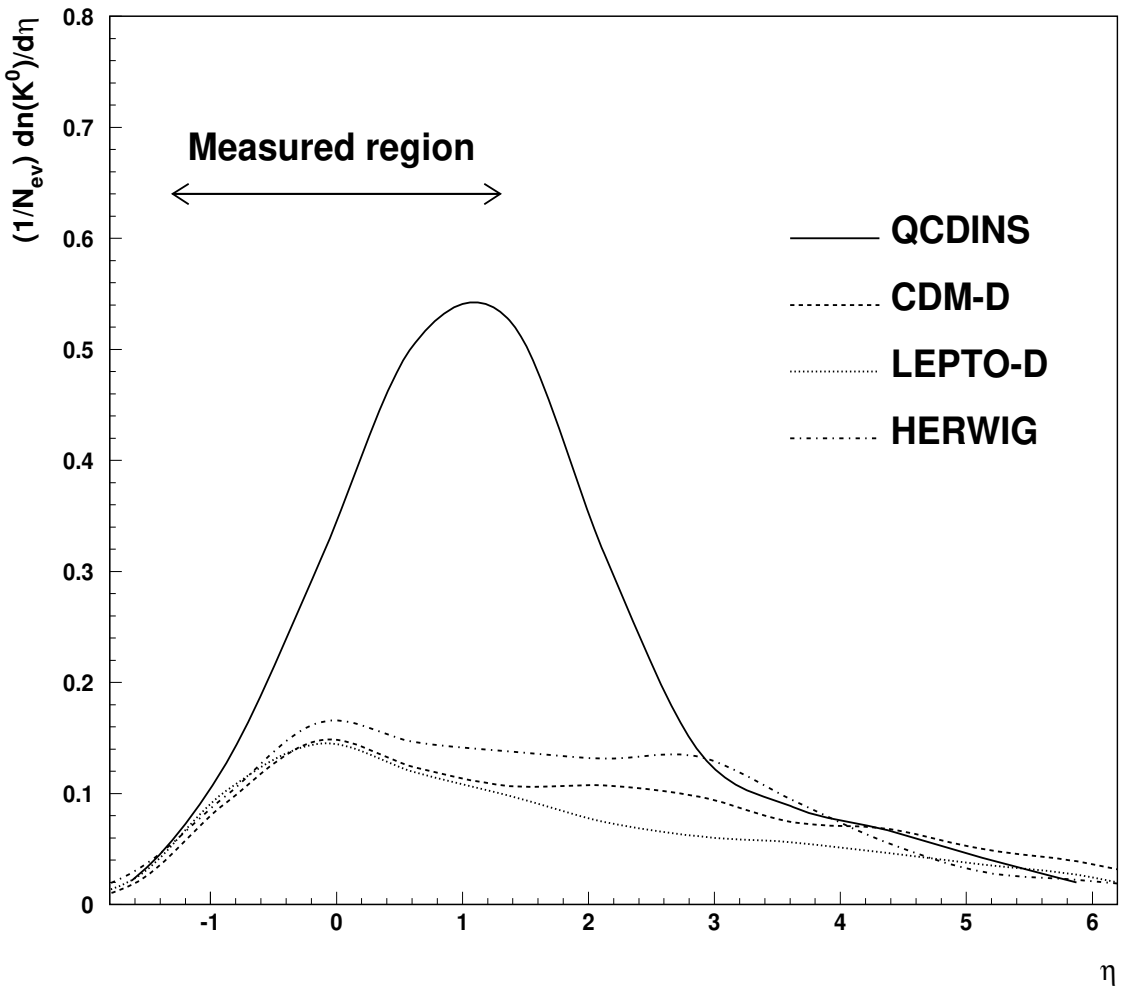

Figure 14: Numbers of K^0 mesons per event with $0.25 < p_T^2 < 4.5\,(\mathrm{GeV/c})^2$ as a function of η for the kinematic region $10 < Q^2 < 70\,\mathrm{GeV}^2$, $10^{-3} < x < 10^{-2}$ and $0.1 < y < 0.6$ predicted by models of non-diffractive DIS (broken lines) and by QCDINS (continuous line).

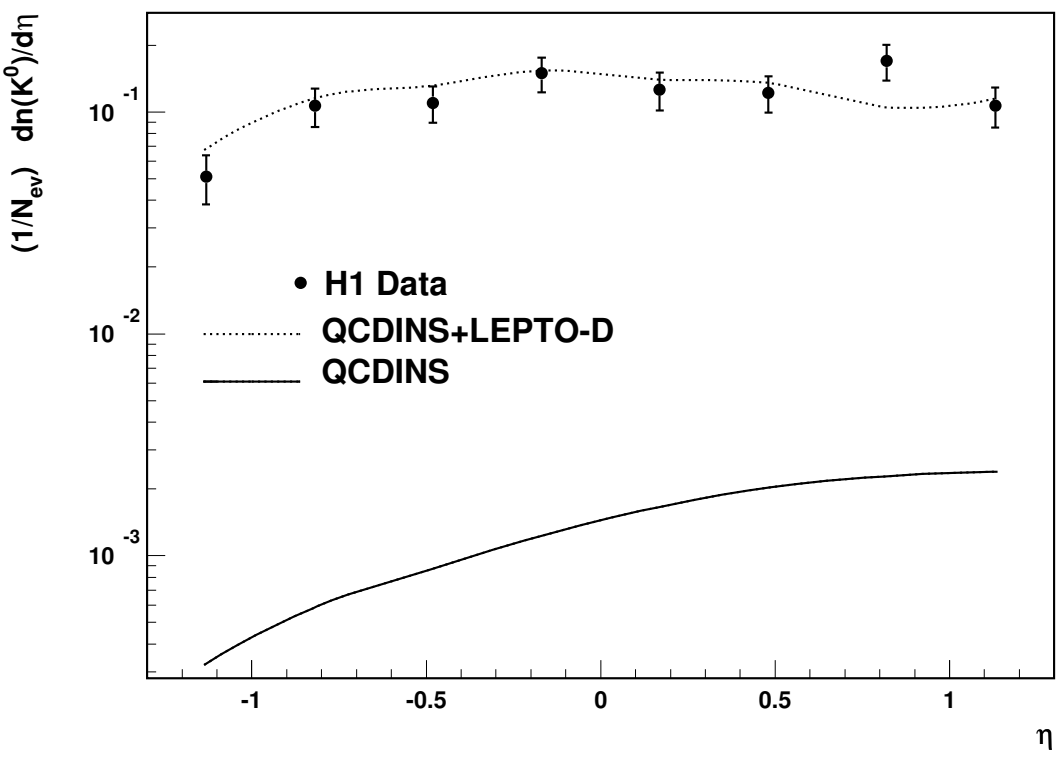

Figure 15: Measured numbers of K^0 mesons per event with $0.25 < p_T^2 < 4.5\,(\mathrm{GeV/c})^2$ for the kinematic region $10 < Q^2 < 70\,\mathrm{GeV}^2$, $10^{-3} < x < 10^{-2}$ and $0.1 < y < 0.6$ (points) with the fit result (dotted line) and the fraction of instanton induced events (solid line), $f = 0.006$, obtained as described in the text; the errors shown are the statistical and systematic errors added in quadrature.

measured in the kinematic region $10 < Q^2 < 70\,\mathrm{GeV}^2$, $10^{-4} < x < 10^{-2}$ and $0.05 < y < 0.6$. No evidence for anomalous sources of strangeness is observed. A reduction of the strangeness suppression factor, λ_s, from the current default value in the JETSET string hadronisation scheme, 0.3, to a value of 0.23 or 0.2 significantly improves the description of the K^0 measurements when using both the LEPTO and CDM Monte Carlo models. This observation is in agreement with the results of previous measurements made in DIS [6, 7] and electron-positron annihilation [11]. The agreement with the latter suggests that the colour forces involved in the hadronisation process are similar in electron-positron annihilation and DIS in the low x region studied here. Further evidence for this is the reasonable description of the measured Λ production rate given by Monte Carlo models using JETSET hadronisation. Such agreement has also been observed in electron-positron annihilation [51], suggesting that the di-quark production mechanisms are similar in both processes.

No evidence is found for differences in the relative rate of strangeness production in diffractive as opposed to non-diffractive DIS, an observation consistent with both the hypothesis that these events result from deep-inelastic positron-pomeron scattering and the hypothesis that they are the product of boson-gluon fusion reactions with subsequent modification of the quark and anti-quark colour charges such that these form a colour singlet.

Direct comparisons of the fractional longitudinal hadronic centre-of-mass momentum ($x_F = 2p_L^*/W$) spectra with previous studies of K^0 and Λ production in DIS [48, 6] at lower energy reveal an increase in the number of particles, particularly at low x_F, as a function of energy. This is expected within the framework of QCD and may be explained as being due to the increased amount of radiation at the higher energy. The x_F spectra are also compared with $x_p = 2p/W$ spectra obtained from a simulation of electron-positron annihilation to u, d and s quarks at the same centre-of-mass energy. These are in good agreement, providing further evidence that the processes involved in the hadronisation in DIS at the low values of x accessible at HERA are the same as those in electron-positron annihilation. A further consequence of the increase in QCD radiation with energy is observed when the mean squared transverse momentum of the K^0 mesons in the hadronic centre-of-mass frame ($\langle p_T^{*2} \rangle$) is studied as a function of x_F. The high energy data are seen to be at higher $\langle p_T^{*2} \rangle$ for a given x_F than the lower energy data [6, 8]. These observations are described well by models of DIS which incorporate QCD effects.

As no evidence for anomalous levels of strangeness production is found, an upper limit of 0.9 nb at the 95% confidence level is placed on the cross-section for QCD instanton induced events in DIS.

10 Acknowledgements

We are grateful to the HERA machine group whose outstanding efforts have made this experiment possible. We appreciate the immense effort of the engineers and technicians who constructed and maintain the H1 detector. We acknowledge the support of the DESY technical staff and thank the DESY directorate for the hospitality extended to the non-DESY members of the collaboration.

References

[1] H1 Collaboration, T. Ahmed *et al.*, Phys. Lett. **B439** (1995) 471.

[2] ZEUS Collaboration, M. Derrick *et al.*, Zeit. Phys. **C65** (1995) 379.

[3] JADE Collaboration, W. Bartel *et al.*, Zeit. Phys. **C20** (1983) 187;
TASSO Collaboration, M. Althoff *et al.*, Zeit. Phys. **C27** (1985) 27;
HRS Collaboration, M. Derrick *et al.*, Phys. Rev. **D35** (1987) 2639;
HRS Collaboration, S. Abachi *et al.*, Phys. Rev. **D41** (1990) 2045;
CELLO Collaboration, H.J. Behrend *et al.*, Zeit. Phys. **C46** (1990) 397;
TASSO Collaboration, W. Braunschweig *et al.*, Zeit. Phys. **C47** (1990) 167;
OPAL Collaboration, G. Alexander *et al.*, Phys. Lett. **B264** (1991) 467.

[4] EMC Collaboration, M. Arneodo *et al.*, Zeit. Phys. **C34** (1987) 283.

[5] B. Andersson, G. Gustafson, G. Ingelman and T. Sjöstrand, Phys. Rep. **97** (1983) 31.

[6] E665 Collaboration, M.R. Adams *et al.*, Zeit. Phys. **C61** (1994) 539.

[7] ZEUS Collaboration, M. Derrick *et al.*, Zeit. Phys. **C68** (1995) 29.

[8] WA21 Collaboration, G.T. Jones *et al.*, Zeit. Phys. **C57** (1993) 197.

[9] WA21 Collaboration, G.T. Jones *et al.*, Zeit. Phys. **C27** (1985) 43.

[10] E632 Collaboration, D. DeProspo *et al.*, Phys. Rev. **D50** (1994) 6691.

[11] DELPHI Collaboration, P. Abreu *et al.*, Zeit. Phys. **C65** (1995) 587.

[12] ALEPH Collaboration, D. Buskulic *et al.*, Zeit. Phys. **C64** (1994) 361.

[13] A.K. Wróblewski, Proceedings of the 25^{th} International Conference on High Energy Physics, Singapore 1990, ed.s K.K. Phua and Y. Yamaguchi, p. 125.

[14] H1 Collaboration, S. Aid *et al.*, Nucl. Phys. **B445** (1995) 3.

[15] ZEUS Collaboration, M. Derrick *et al.*, Zeit. Phys. **C67** (1995) 93.

[16] H1 Collaboration, S. Aid *et al.*, Phys. Lett. **B358** (1995) 412.

[17] A. Ringwald and F. Schrempp, DESY-94-197 (1994);
M.J. Gibbs, A. Ringwald and F. Schrempp, DESY-95-119 (1995).

[18] Yu. L. Dokshitzer, Sov. Phys. JETP **46** (1977) 641;
V.N. Gribov and L.N. Lipatov, Sov. J. Nucl. Phys. **15** (1972) 438 and 675;
G. Altarelli and G. Parisi, Nucl. Phys. **126** (1977) 297.

[19] E.A. Kuraev, L.N. Lipatov and V.S. Fadin, Sov. Phys. JETP **45** (1977) 199;
Y.Y. Balitsky and L.N. Lipatov, Sov. J. Nucl. Phys. **28** (1978) 282.

[20] A.J. Askew, J. Kwieciński, A.D. Martin and P.J. Sutton, Phys. Lett. **B325** (1994) 212;
H1 Collaboration, S. Aid *et al.*, Phys. Lett. **B354** (1995) 494.

[21] J. Kwieciński, A.D. Martin, P.J. Sutton and K. Golec-Biernat, Phys. Rev. **D50** (1994) 217; K. Golec-Biernat, J. Kwieciński, A.D. Martin and P.J. Sutton, Phys. Lett. **B335** (1994) 220.

[22] H1 Collaboration, S. Aid *et al.*, Phys. Lett. **B356** (1995) 118.

[23] DELPHI Collaboration, P. Abreu *et al.*, Zeit. Phys. **C67** (1995) 543.

[24] H1 Collaboration, T. Ahmed *et al.*, Phys. Lett. **B348** (1995) 681.

[25] ZEUS Collaboration, M. Derrick *et al.*, Zeit. Phys. **C68** (1995) 569.

[26] J.P. Philips, Proceedings of the International Workshop on Deep Inelastic Scattering and Related Topics, Paris, France, 1995, ed.s J-F. Laporte and Y. Sirois, in litt.

[27] ZEUS Collaboration, M. Derrick *et al.*, Phys. Lett. **B356** (1995) 129.

[28] W. Buchmüller, Phys. Lett. **B353** (1995) 335;
W. Buchmüller and A. Hebecker, Phys. Lett. **B355** (1995) 573.

[29] H1 Collaboration, DESY Internal Report, DESY H1 96-01, March 1996.

[30] H1 Calorimeter Group, B. Andrieu *et al.*, Nucl. Instr. and Meth. **A336** (1993) 460.

[31] J. Ban *et al.*, Nucl. Instr. and Meth. **A372** (1996) 399.

[32] H1 Collaboration, T. Ahmed *et al.*, Zeit. Phys. **C66** (1995) 529.

[33] G. Ingelman, "LEPTO Version 6.1: The Lund Monte Carlo for Deep Inelastic Lepton-Nucleon Scattering", Proceedings of the Workshop on Physics at HERA, Hamburg 1991, editors W. Buchmüller and G. Ingelman, Vol. 3, p. 1366.

[34] L. Lönnblad, Comp. Phys. Comm. **71** (1992) 15.

[35] M. Seymour, Comp. Phys. Comm. **67** (1993) 465.

[36] A.D. Martin, W.J. Stirling and R.G. Roberts, "MRS Parton Distributions", Proc. of the Workshop on Quantum Field Theoretical Aspects of High Energy Physics, editors B. Geyser and E.M. Ilgenfritz (1993), p. 11;
A.D. Martin, W.J. Stirling and R.G. Roberts, Phys. Rep. **97** (1983) 31.

[37] H1 Collaboration, T. Ahmed *et al.*, Phys. Lett. **B407** (1993) 515.

[38] ZEUS Collaboration, M. Derrick *et al.*, Phys. Lett. **B316** (1993) 412.

[39] T. Sjöstrand, Comp. Phys. Comm. **82** (1994) 74.

[40] B. Andersson, G. Gustafson and L. Lönnblad, Nucl. Phys. **B339** (1990) 393.

[41] K. Charchula, G. Schuler and H. Spiesberger, Comp. Phys. Comm. **81** (1994) 381.

[42] A. Kwiatkowski, H. Spiesberger and H.-J. Möhring, Comp. Phys. Comm. **69** (1992) 155.

[43] H. Jung, Comp. Phys. Comm. **86** (1995) 147.

[44] Talk given by A. Mehta at the Topical Conference on Hard Diffraction, Eilat, Israel, February 1996;
S. Taprogge, to appear in the Proceedings of the XXXI Rencontre de Moriond, Les Arcs, France, March 1996, ed. J. Trân Thanh Vân.

[45] M.J. Gibbs, A. Ringwald, B.R. Webber and J.T. Zadrozny, Zeit. Phys. **C66** (1995) 285.

[46] L. Montanet *et al.*, Phys. Rev. **D50** (1994) 1173.

[47] L. Lönnblad, Zeit. Phys. **C65** (1995) 285;
A.H. Mueller, Nucl. Phys. **B415** (1994) 373;
L. Lönnblad, CERN-TH/95-095.

[48] EMC Collaboration, M. Arneodo *et al.*, Phys. Lett. **B150** (1985) 458.

[49] H1 Collaboration, I. Abt *et al.*, Zeit. Phys. **C63** (1994) 377.

[50] A. Ringwald, F. Schrempp and M. Gibbs, to appear in the Proceedings of the International Workshop on Deep Inelastic Scattering and Related Phenomena, Rome, Italy, April 1996, ed. G. D'Agostini.

[51] DELPHI Collaboration, P. Abreu *et al.*, Phys. Lett. **B318** (1993) 249.